

Xenon NMR as a probe for microporous and mesoporous solids, polymers, liquid crystals, solutions, flames, proteins, imaging

Kristin Bartik, Philippe Choquet, André Constantinesco, Guillaume Duhamel, Jacques Fraissard (coord.), Jean-Noël Hyacinthe, Jukka Jokisaari, Emanuela Locci, Thomas J. Lowery, Michel Luhmer, Thomas Meersmann, Igor L. Moudrakovski, Galina E. Pavlovskaya, Kimberly L. Pierce, Alexander Pines, John A. Ripmeester, Ville-Veikko Telkki, Wibren S. Veeman

Abstract We present in this paper some examples of the applications of the Nuclear Magnetic Resonance (NMR) of xenon used as a probe in the study of different chemical environments: determination of the porosity of micro- and mesoporous solids, evaluation of the concentrations and sizes of amorphous domains in solid polymers, characterization of liquid crystals, study of combustion processes at high temperature, determination of the structure and dynamics of organic systems and proteins in solution, assessment of cerebral blood flow.

Keywords Xenon NMR, porous solids, liquid crystals, polymers, proteins, imaging.

Résumé RMN du xénon adsorbé utilisé comme sonde pour l'étude de solides micro- et mésoporeux, polymères, cristaux liquides, solutions, flammes, protéines et pour l'imagerie

Ce papier donne quelques exemples d'applications de la résonance magnétique nucléaire (RMN) du xénon utilisé comme sonde à l'étude de divers systèmes chimiques. Citons, de façon non exhaustive : la détermination de la porosité des solides micro- et mésoporeux, l'évaluation de la concentration et des dimensions des domaines amorphes dans les polymères solides, la caractérisation des cristaux liquides, l'étude des processus de combustion à haute température, la détermination de la structure et de la dynamique des systèmes organiques et de protéines en solution, l'estimation du débit sanguin dans le cerveau.

Mots-clés RMN du xénon, solides poreux, cristaux liquides, polymères, protéines, imagerie.

The fundamental idea was to find a chemically inert molecule, particularly sensitive to physical interactions with other species, which could be used as a probe to determine the properties of its environment. This probe needed to be, moreover, detectable by Nuclear Magnetic Resonance (NMR) since this technique is particularly well adapted to the study of the electronic perturbations of molecules under-going rapid movement.

Xenon is this ideal probe. It is an inert, monoatomic gas, with a very large, spherically symmetrical electron cloud. Any distortion of this latter is felt directly at the level of the nucleus and is consequently expressed as a variation of the xenon NMR parameters. From the NMR point of view, the ^{129}Xe isotope is particularly suitable: it has a spin $1/2$, its natural abundance is 26%, its detection sensitivity is good (ca. 10^{-2} that of the proton), and it presents a large chemical shift range. Despite its lower sensitivity, the ^{131}Xe isotope (spin $3/2$) is, due to its large nuclear moment, essentially used for relaxation and electric field gradient measurements.

Chemical shifts and relaxation times of xenon are solely affected by intermolecular interactions and are exquisitely sensitive to the atom's surrounding. This sensitivity to its environment permits the Xe nucleus to report on a wide

variety of attributes of the physical systems in which it finds itself: gas, liquid, cage in a zeolite, nanochannel in a molecular solid, clathrate, protein in solution, amorphous polymer, etc. It can be used also for imaging and gas diffusion measurements. Several reviews have been published on these applications [1-4]. By using optical polarization techniques [5] the sensitivity of detection can be increased by several orders of magnitude, which widens the field of applications of this technique. The use of a continuous flow approach [6] for the production of hyperpolarized xenon (denoted HP Xe in this text) is particularly beneficial for several applications (porous materials [7], flames [8], microimaging [9], etc.). We present some examples of the applications of the Xe NMR technique to different environments.

^{129}Xe NMR spectroscopy in microporous materials (zeolites)

Zeolites are currently among the most important silico-aluminate compounds used in industry, especially in catalysis [10]. Their general formula is $\text{C}_{x/n}(\text{AlO}_2)_x(\text{SiO}_2)_y \cdot m\text{H}_2\text{O}$. The negative charge on the lattice, equal to the number of Al atoms, is compensated by exchangeable cations C^{n+} . Zeolites

have porous structures consisting of cavities and/or channels of molecular dimensions where the cations and adsorbed molecules are located. The form and the dimensions of the pores are important parameters since they can affect the specificity of these catalysts.

Many defects or properties of zeolite-based catalysts are difficult to detect by classical physicochemical methods, for example: pore dimensions, short range crystallinity and structural defects, the size of very small supported metal particles when they are too small to be detected by electron microscopy, etc.

The essential information is obtained from the analysis of the variation of the chemical shift with the xenon concentration (denoted [Xe] or N atoms/g of solid) and the experiment temperature T. This curve is characteristic of each zeolite (figure 1). It has been shown that the chemical shift, δ , of adsorbed xenon is the sum of several terms corresponding to the various perturbations it suffers [11].

$$\delta(T) = \delta_{\text{ref}} + \delta_S + \delta_{\text{Xe}} + \delta_{\text{SAS}} + \delta_E + \delta_M \quad (1)$$

δ_{ref} is the reference (gaseous xenon at zero pressure). δ_S arises from interactions between xenon and the surface of the zeolite pores, provided that the solid does not contain any electrical charges. $\delta_{\text{Xe}} = \delta_{\text{Xe-Xe}} \rho_{\text{Xe}}$ corresponds to Xe-Xe interactions; it increases with the local density, ρ_{Xe} , of adsorbed xenon and becomes predominant at high xenon pressure. When the Xe-Xe collisions are isotropically distributed (large spherical cage), the relationship $\delta = f[N]$ is a straight line (figure 1). The slope, $d\delta/dN$, is proportional to the local xenon density and, therefore, inversely proportional to the « void volume ». If the Xe-Xe collisions are anisotropically distributed (narrow channels), the slope of this function increases with N (figure 1).

When there are strong adsorption sites (SAS) in the void space with which xenon interacts much more strongly than with the cage or channel walls, each xenon spends a relatively long time on these SAS, particularly at low xenon concentration. The corresponding chemical shift, δ , will be greater than in the case of a non-charged structure (figure 2). When N increases, δ must decrease if there is fast exchange of the atoms adsorbed on SAS with those adsorbed on the other sites. When N is high enough, the effect of Xe-Xe interactions becomes again the most important and the dependence of δ on N is then similar to that in (figure 1). In

this case the chemical shift extrapolated to zero concentration, $\delta_{N \rightarrow 0}$, depends on the nature, the number, the charge (effect of the electric field, δ_E) and the paramagnetism (δ_M) of these strong adsorption sites. One exception to this variation should be noted: cations with electronic structure d^{10} and small charge (Cu^+ and Ag^+) reduce δ , which can even become negative. This is due to the overlap of the d^{10} orbital of the cations and the d^0 of Xe during the lifetime of the cation-Xe van der Waals complex. This technique proves to be the most simple for detecting Cu^+ . Sometimes strong adsorption sites of different types (for example, various highly charged cations or metal particles) are distributed in solid pores. If the exchange of Xe between these various sites is fast with respect to the NMR chemical shift time-scale, an average signal is observed, while several lines correspond to a situation of slow exchange [11].

The δ_S term, characteristic of Xe-surface interactions, has been related to the dimensions and the shape of the pores, and to the ease of diffusion of the Xe atom in the free space; more precisely to the mean free path, \bar{l} , of a Xe atom inside the pore volume, defined as the average distance travelled by a Xe atom between two successive collisions with the pore walls [12]. To explain the hyperbolic relation obtained between δ_S and \bar{l} for various zeolites (figure 3)

$$1/\delta_S = (1/\delta_a) (1 + \bar{l}/a) \quad (2)$$

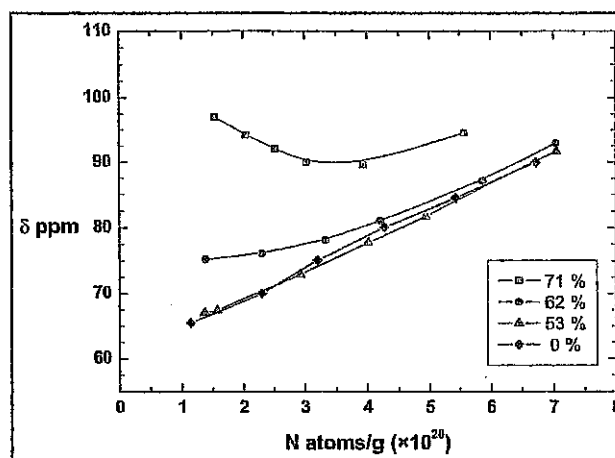


Figure 2 - Chemical shift variation versus xenon concentration for HY zeolite (straight line) and for MgY zeolite for various Mg^{2+} content.

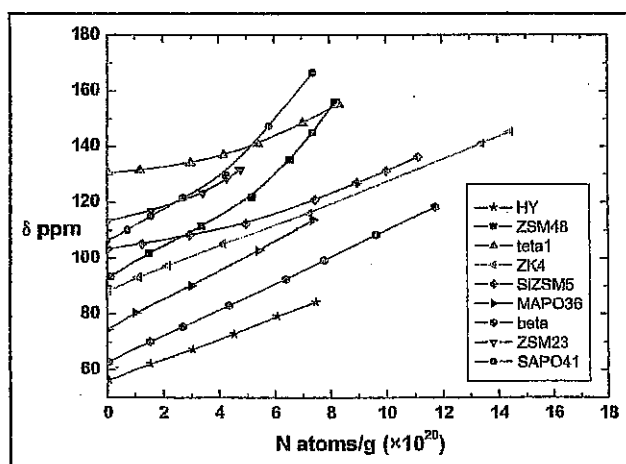


Figure 1 - Dependence of the chemical shift δ on the concentration of adsorbed xenon per gramme of zeolite.

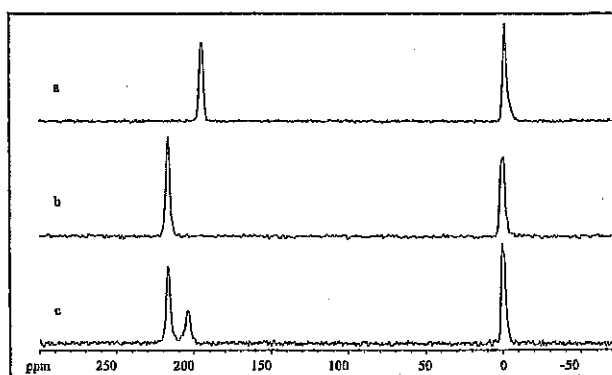


Figure 3 - Variation of δ_S against the mean free path \bar{l} calculated for several zeolites.

a simple model of fast site exchange has been used ($a = 0.2054 \text{ \AA}$ δ_a depends on the surface curvature, hence on r). Other physisorption models have been proposed [14-15].

At 300 K, which is the usual recording temperature, δ_s is the average value of the shift of one isolated xenon in rapid exchange between a position A on the pore surface [defined by δ_a which depends on Xe-surface interactions [16] and a position in the volume V of the pore (defined by δ_v with $\langle \delta_v \rangle = f(\delta_a, \bar{r})$].

$$\delta_s = (n_a \delta_a + n_v \delta_v) / (n_a + n_v) \quad (3)$$

n_a and n_v are the probabilities of there being a Xe atom at the surface (A) or in the volume (V). The effect of a decrease in the experiment temperature increases with \bar{r} and provides another way of determining the pore size.

In the 1980s, this technique allowed the determination of the free spaces in zeolites without knowing their structure [17]. Today it is much more often used:

- to demonstrate the presence of different pores in the same zeolite, and in some cases the intergrowth of structures difficult to quantify by X-ray diffraction;
- to reveal structural defects produced, for example, by dealumination of zeolites, and to determine their characteristics [11b];
- to locate cations in the pore structure and to follow their migration in the same crystallite or between different crystallites, and/or valence change (for example, Cu^{2+} , Cu^+ and Cu^0) as a function of different factors. To demonstrate also the blockage of certain types of pore by cations, and the resulting effect on the rate of exchange between the different zones [18];
- to study the flexibility of structure as a function of temperature [19];
- to locate any « encumbering » species; for example: adsorbed molecules, extra-framework species, coke formed during a catalytic cracking reaction, etc. [4];
- to determine the size of metal particles supported on zeolites (especially when they are too small to be seen by electron microscopy), their location in the crystallite and the distribution of the molecules chemisorbed or not on these particles (as opposed to the mean coverage) [4];
- in some cases to detect the formation of bimetallic particles [4];
- to follow the diffusion of hydrocarbons in a zeolite and to determine their inter- and intracrystallite diffusion coefficients [4].

We mention also the interest of ^{131}Xe NMR of the 131 isotope for the quantification of the electric field in zeolite pores [20].

^{129}Xe NMR spectroscopy in mesoporous materials

The porosity of numerous materials of industrial and scientific importance, particularly catalysts and sorbents, extends well into the mesopore region, with pore diameters of $\sim 20\text{-}500 \text{ \AA}$. Often such materials are also either amorphous or poorly crystalline, which limits the applications of diffraction-based methods. After many successful applications of Xe NMR to crystalline microporous materials (pore diameters $\leq 20 \text{ \AA}$) in the 1980s and early 1990s, naturally there has been a growing interest in the application of this technique to such porous materials, especially with the use of HPXe [7, 21-23].

Before a discussion of the known applications, it would be useful to consider some specifics of Xe NMR

spectroscopy to mesoporous systems. Very large and easily accessible pores, plus fast diffusion of xenon, cause exchange to have pronounced effects on the observed spectra. In the case of weak interactions with the surface, which is often so for xenon in mesoporous materials, the adsorption is described by Henry's law. In such a situation the observed chemical shift of xenon can be expressed as [24-25]:

$$\delta = \frac{\delta_g}{1 + (V_g / KSRT)} \quad (4)$$

where S is the specific surface area, V_g is the free volume inside the adsorbent, K is the Henry's law constant, δ_s stands for the chemical shift of surface-adsorbed Xe atoms, R is the universal gas constant, and T is the temperature. The equation shows that the observed shift is expected to be independent of the xenon pressure. This is commonly observed in experiments, at least at low pressures when Xe-Xe interactions are insignificant and the adsorption indeed follows Henry's law. Equation (4) shows that the chemical shift δ also depends strongly on S/V_g , the surface-to-volume ratio of the pores occupied by Xe atoms involved in fast exchange. It is therefore expected that the spectra of materials with a distribution of S/V_g will reflect this feature either by the appearance of more than one line, or by the presence of a broad line. The presence of small particles (less than about $10 \mu\text{m}$) in the material studied will also result in broad lines [25-26]. Specifically, the effects of xenon exchange and bulk properties of porous materials on the spectra have been demonstrated and discussed in terms of xenon diffusion path length using 40 \AA Vycor controlled-pore glass of different particle sizes [26]. According to equation (4), the mean pore size D related to the V_g/S as $D = \eta V_g/S$ (η is a parameter dependent on the pore shape), can be found from the NMR experiment provided that K is known from adsorption experiments. The correlation of the observed chemical shift with D (figure 4) as obtained by conventional adsorption methods has uncovered a general correlation between δ and D of the form $\delta = \delta_g / (1 + D/b)$ [25-27] that is similar to those found for zeolites [12].

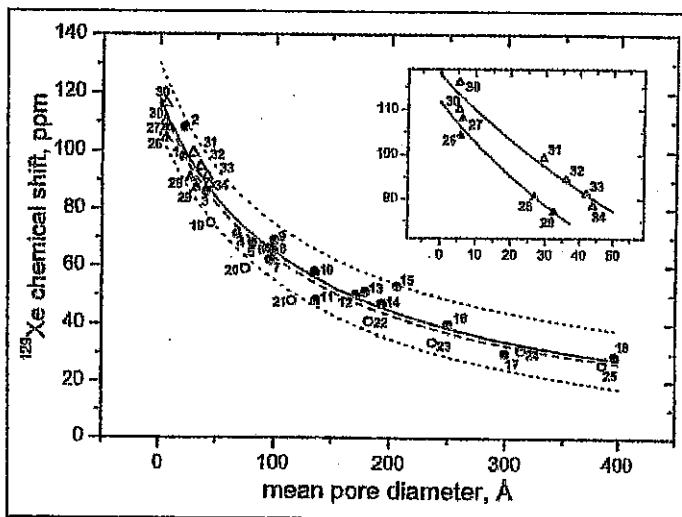


Figure 4 - ^{129}Xe chemical shifts vs mean pore diameters for porous silica-based materials: • silica gels; ○ Vycor/CPG; ▲ and △ porous organo-silicates of two different origins.

The solid curve is the nonlinear least-squares fit for samples 1-18, with prediction bands given at a confidence level of 95% shown as the dotted curves. The dashed curve is the fit for all samples. Inset: fits for two subsets of porous organo-silicates.

For 34 silica-based materials with pores in the range of 0.5–40 nm, the parameters of the equation obtained from the fit are $\delta_g = 116 \pm 3$ ppm and $b = 117 \pm 8$ Å [27]. With some caution, the correlation can be used for the characterization of silica samples with unknown pore structure. One needs to note that even within this general correlation, subsets of materials of similar origin display yet finer correlations that indicate an acute sensitivity of the method to details of the pore structure.

Temperature-dependent chemical shift data can be used to extract the physical parameters related to the adsorption properties of materials. In the fast exchange approximation with weak adsorption, as described by Henry's law, the temperature dependence of the observed xenon chemical shift δ for arbitrary pores can be expressed as [25]:

$$\delta = \delta_g \left(1 + \frac{V_g}{V_0 S R T^{1/2}} e^{\frac{\Delta H_{ads}}{RT}} \right)^{-1} \quad (5)$$

The heat of adsorption ΔH_{ads} can be found by fitting the experimental temperature dependence of the chemical shift and, for Xe physically adsorbed on silica-based surfaces, can range from just a few kJ/mol to about 20 kJ/mol [25]. If the pre-exponent of the Henry's constant is known from independent adsorption measurements, then the V_g/S ratio can be found as well. Application of equation (5) necessitates working at very low xenon concentrations to reduce the effects of Xe-Xe interactions and to prevent Xe condensation in the pores at low temperature.

A very interesting class of mesoporous materials with regularly spaced and uniformly sized pores [28] was introduced in the early 1990s. The silica-based forms of such materials as MCM-41, MCM-48, SBA-15 etc. received perhaps the most attention in ^{129}Xe NMR studies [29–37]. These materials can be prepared with pores in a very broad range of sizes and are a good testing ground for the chemical shift-pore size correlations. The first studies demonstrated [29–30], however, that the observed shifts could fall well outside the range predicted by the general correlations obtained for silicates [25–27]. In most cases, the chemical shift of adsorbed xenon is practically independent of the xenon pressure, and the observed values are almost always below those estimated from the empirical correlations. Since the materials are prepared as very fine powders with the particle size rarely exceeding 10 μm , the exchange between adsorbed and gas phases is expected to contribute heavily to the observed shifts. Indeed, compression of the samples [30] produced significant downfield shifts similar to those in compressed aerosils [24] or in Vycor porous glass with different particle sizes [26].

In a recent study [32], the NMR of continuously circulating hyperpolarized Xe has been used to characterize purely siliceous and ordered Al-containing mesoporous MCM-41 and SBA-15. The effect of compression on the mesopore structure has also been studied. The NMR spectra obtained can be interpreted in terms of exchange between adsorbed xenon in the pores and gaseous Xe atoms in the interparticle spaces. The greatly increased sensitivity arising from hyperpolarized Xe has also been used to detect the spectra of xenon adsorbed on very small quantities of mesoporous silica thin films [36].

Additional information about internal surface of the pores can be obtained from the data on co-adsorption of Xe with some other small molecules [29–31, 35]. The co-adsorption

studies can be particularly useful for screening intra-wall micropores, surface defects and inhomogeneities in porosity. In certain cases, using guest molecules of different sizes, it is possible to distinguish and estimate the sizes of micropores inside the mesoporous walls [35].

The assessment of the distribution and accessibility of moieties attached to the walls of mesoporous silicates is another area of ^{129}Xe NMR applications. The effects of hydrocarbon chains attached to the silica walls has been the subject of an extensive hyperpolarized ^{129}Xe NMR study [7]. The variable temperature measurements revealed a non-uniform porosity and irregular pore structure, and allowed one to follow the changes in the adsorption properties of xenon due to modification of the mesopore voids [7]. In another study [37], the presence of Pt in the ordered mesoporous silicates results in a notable chemical shift of adsorbed xenon. It was concluded that the Pt clusters are situated inside the pores of the mesoporous molecular sieve rather on the external surface.

There are a number of Xe NMR reports dealing with rather less traditional mesoporous materials. The application of Xe NMR spectroscopy to the characterization of soil meso- and microporosity has been demonstrated in [38]. Based on the analysis of the spectra, a model for the possible mutual location of organic matter and iron compounds in natural soils was suggested. Another study used hyperpolarized Xe to characterize the hierarchically ordered positive and negative replicas of wood cellular structures prepared using surfactant templating methods [39]. Xe NMR data confirm a highly ordered and uniform structure with interconnected porosity in the positive silica wood replicas prepared under acidic conditions. In contrast, non-uniform porosity with irregular pore structures is inferred from similar data for negative silica wood replicas prepared under basic conditions [39].

Aerogels of different natures represent an important class of open-pore mesoporous materials with extremely low framework density, reaching values as low as 0.05 g/cm³ and possessing great potential for various industrial applications. A recent ^{129}Xe NMR study of aerogels [40], performed as a combination of spectroscopic and spatially resolved NMR spectroscopy, has proved to be a powerful approach for characterizing the average pore structure and steady-state spatial distribution of xenon atoms in different physicochemical environments. The method offers unique information and insights into the microscopic morphology of aerogels, the dynamical behavior of adsorbates, and provides spatially resolved information on the nature of the defect regions found in these materials [40]. The extremely low density of aerogels, however, required very long accumulations (often in excess of 20 hours). The problem of long experimental data acquisition times was addressed in another study by employing the Xe-131 isotope and a very high density of xenon [41].

A more practical approach to obtain the Xe NMR spectra of aerogels is to employ the high sensitivity of HP Xe. Application of NMR microimaging using continuous flow HP Xe resulted in a visual picture of the dynamics of gases inside the particles of aerogels [9]. The produced « polarization-weighted » images of gas transport in aerogel fragments are correlated to the diffusion coefficient of xenon obtained from NMR pulsed-field gradient experiments. In another diffusion-related study [21], the ingress of HP Xe in Vycor porous glass was followed by 1D NMR imaging and by observing the intensity of the NMR signal. The resulting

diffusion coefficients compared well with the results obtained from the pulsed field gradient measurements with thermally polarized Xe.

In a more recent report [23], HP Xe NMR has been used to probe the geometry and interconnectivity of pores in resorcinol-formaldehyde aerogels of different preparations and to correlate them with the [resorcinol]/[catalyst] (*R/C*) ratios used in the preparation.

It has been demonstrated that variable temperature HP ^{129}Xe -NMR can be used for accurate measurement of the volume-to-surface-area (V_g/S) ratios in these organic mesoporous materials. 2D NMR measurements revealed a hierarchical exchange process between the gas phase xenon, xenon adsorbed in mesoporous regions and Xe in microporous regions of the aerogels. In the aerogels studied, the exchange of Xe gas follows the sequence (from fastest exchange to slowest): mesopore with free gas, gas in meso- and micropores, free gas with micropores and, finally, among micropore sites (figure 5a-c). The homogeneity of the distribution of mesopores in the aerogels was checked

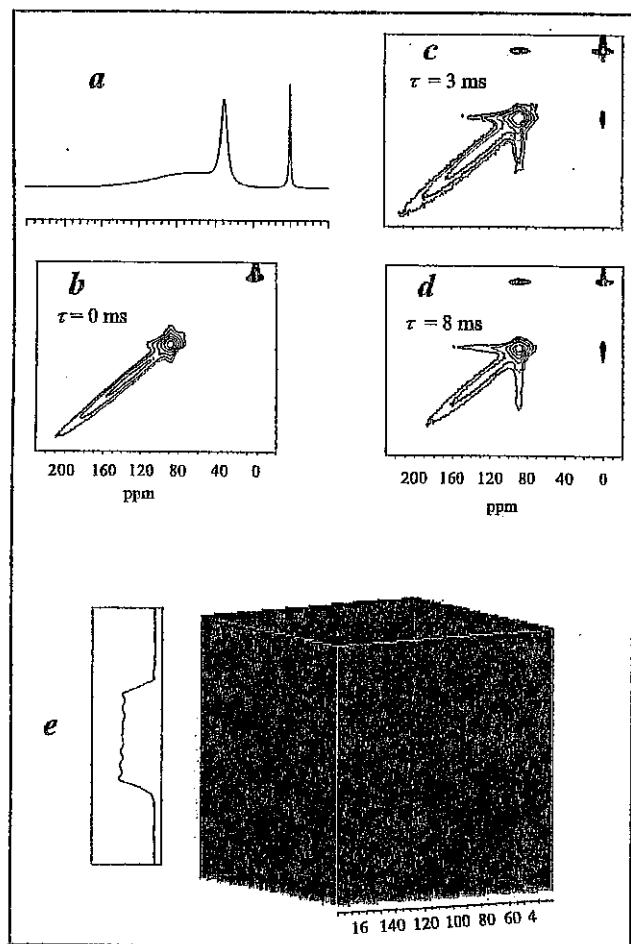


Figure 5 - (a) CF HP ^{129}Xe NMR spectra for aerogels prepared with an *R/C* ratio of 300. Signals of free gas at 0 ppm, gas in meso- (ca 100 ppm) and micropores; (b-d) CF HP 2D EXSY ^{129}Xe NMR spectra for aerogels (*R/C* = 300) recorded as indicated. All spectra were obtained at 293 K with a HP Xe flow rate of 45 standard cubic centimeters per minute (sccm); (e) CF ^{129}Xe chemical shift image of Xe in cylindrical block of aerogel (*R/C* = 300). Intensity profile shown on the left is taken through the center of the image.

directly using CF ^{129}Xe Chemical Shift Imaging (figure 5e). The evenness of the image profile clearly indicated the uniformity of the distribution of the mesoporous space throughout the bulk of the aerogel.

Xe NMR cryoporometry

NMR cryoporometry is a method in which ^1H NMR of an organic substance confined in porous materials is used for the determination of the pore size distribution [42]. The substance in a small pore has a lower melting point than the bulk substance. According to the Gibbs-Thompson equation [43], the melting point depression ΔT is inversely proportional to the pore radius R_p :

$$\Delta T = T_0 - T = \frac{k_p}{R_p} \quad (6)$$

Here T_0 is the bulk melting temperature, T is the melting point in a pore of radius R_p , and k_p is a constant, characteristic of each probe liquid. In NMR cryoporometry, the melting point temperature distribution is detected through the intensity variation of the ^1H resonance of the unfrozen component of the confined substance, and the pore size distribution is calculated by using equation (6).

Xenon porometry is a novel method for the determination of pore dimensions. It has been developed on the basis of NMR cryoporometry. In this method, a porous material is immersed in an organic substance, and the freezing and melting behaviors of the substance are explored by means of the ^{129}Xe NMR spectroscopy of xenon dissolved in the sample [44]. An example of the spectra measured at different temperatures is shown in figure 6. The signals have been labeled in the figure.

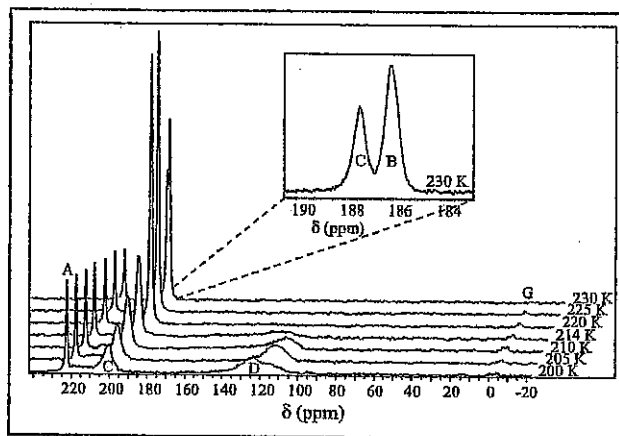


Figure 6 - ^{129}Xe NMR spectra of the sample containing silica gel 100, acetonitrile and xenon at different temperatures.

The measurement temperatures are shown beside the spectra. The chemical shift range of the signals B and C at 230 K has been expanded in the inset of the figure.

The origins of the components are the following: *signal A* arises from the inner xenon thermometer, which is a capillary tube in the middle of a 10 mm sample tube containing ethyl bromide and xenon gas [45]. *Signals B and C* originate from xenon dissolved in the liquid substance. *Signal B* arises from bulk substance located in the spaces between particles of porous material and on the top of porous material, and

vanishes below the freezing temperature of the substance (227 K in the case of acetonitrile), as the transition from liquid to solid is accompanied by an abrupt reduction of gas solubility. *Signal C* originates from liquid inside the pores, and gradually vanishes at lower temperatures, as the confined substance freezes. If the density of the substance increases substantially (as occurs in the case of acetonitrile), *signal D* appears at lower temperatures. This signal arises from xenon in very small gas bubbles appearing inside the pores. The bubbles build up during the freezing of confined substance, as the substance contracts. The signal vanishes, as the confined substance melts. As bulk substance freezes, bubbles also build up in between the particles of porous materials due to the density change, and *signal G* originates from xenon in this environment. Since the bubbles are much bigger than those inside the pores, the chemical shift of *signal G* is close to that of bulk gas.

The method provides three novel possibilities for determining pore sizes:

1) As, on one hand, the melting point of the bulk substance can be deduced from the emergence of *signal B* and from the disappearance of *signal G*, and, on the other hand, the disappearance of *signal D* and the changes of the intensity of *signal C* reveal the lowered melting point of the confined substance, the melting point depression can be determined by measuring the NMR spectra at variable temperature, and the average pore size of the material can be calculated by the Gibbs-Thompson equation in the same way as in the usual NMR cryoporometry.

2) The chemical shift difference of *signals C* and *B* is dependent on pore size. By determining the correlation for a certain substance at a certain temperature using known mesoporous materials, the pore size of an unknown sample material can be measured. This is very easy to do, because the signals can be recorded by a single scan measurement at any temperature above the bulk melting point. On the other hand, the correlation is quite inaccurate because the line-width of the signals is large compared to the distance between them. The correlation is best suited for pore size determination of smaller pore sizes in the mesoporous range.

3) As the size of the gas bubbles formed inside the pores during the freezing of the confined substance depends on the size of the pores, the chemical shift of xenon atoms inside the bubbles also depends on the pore size. These studies prove that the large majority of bubbles are isolated (i.e. they are not connected with each other) giving resonance signals characteristic of each pore size. As *signal D* is made up of these components, the shape of the signal represents the pore size distribution. The correlation between the chemical shift of *signal D* and the pore size can be determined using known reference samples. After that, the pore size distribution of an unknown material can be determined by measuring its NMR spectrum [44].

Liquid crystals as studied by Xe NMR spectroscopy

Liquid crystals (LC) can be classified into two main categories: thermotropic (TLC) and lyotropic (LLC) liquid crystals. The TLCs are usually formed by rod- or disk-like molecules and display liquid-crystalline phases (mesophases) within a certain temperature range. At higher temperatures, a transition to the isotropic phase takes place and at lower tempera-

ture to the solid state. The mesophases of TLCs can further be divided, for example, into nematic, smectic A and smectic C phases according to the orientational order of molecules. In the nematic phases, there is long-range orientational order but no positional order. The molecules, however, tend to orientate in a common direction which defines the direction of the LC director, \mathbf{n} . In smectic A and C phases, the LC molecules possess also positional order leading to a layer structure. The director \mathbf{n} is parallel to the layer normal in smectic A phases. On the contrary, in smectic C phases, the director is tilted with respect to the layer normal. The structures of these phases are illustrated in figure 7. Lyotropic phases are formed by mixing various compounds, one of them usually being water. TLCs are very important compounds in display technology. Therefore, the knowledge of their physical properties is extremely important. A very significant property is the response time which shows how quickly the LC reacts to external disturbances, such as electric and magnetic fields. A class of LCs which has particular potential in display technology is chiral LCs which possess ferroelectric phases. In recent investigations of three-dimensional protein structures by NMR so-called dilute liquid crystalline solutions are applied. These consist of, for example, water and micelles at variable concentrations [46]. A detailed description of liquid crystals can be found in [47].

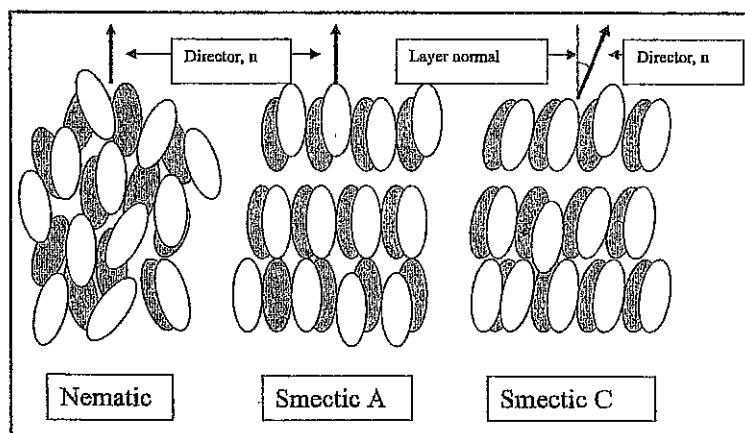


Figure 7 - Schematic illustration of a nematic, smectic A and smectic C phase. Director \mathbf{n} indicates the average orientation of molecules. In the smectic A phase, \mathbf{n} is parallel with the layer normal whereas in the smectic C phase it is tilted with respect to the layer normal. The tilt angle is dependent upon temperature.

The first ^{129}Xe NMR experiments of xenon in TLCs were published in 1987 [48]. Since those days, the Xe NMR of xenon in LCs has developed to a level that allows the determination of many properties, as will be discussed below.

When a liquid-crystalline sample is placed in a magnetic field \mathbf{B} , the LC director \mathbf{n} orients either parallel with or perpendicular to \mathbf{B} , depending upon the sign of the anisotropy of macroscopic diamagnetic volume susceptibility of LC, $\Delta\chi_d$: if $\Delta\chi_d > 0$, then $\mathbf{n} \parallel \mathbf{B}$, and if $\Delta\chi_d < 0$, then $\mathbf{n} \perp \mathbf{B}$. This is clearly seen in figure 8 which shows the ^{129}Xe shielding as a function of temperature in different TLCs. Another feature that is obvious from figure 7 is the fact that ^{129}Xe NMR experiments of xenon in TLCs reveal phase transition temperatures.

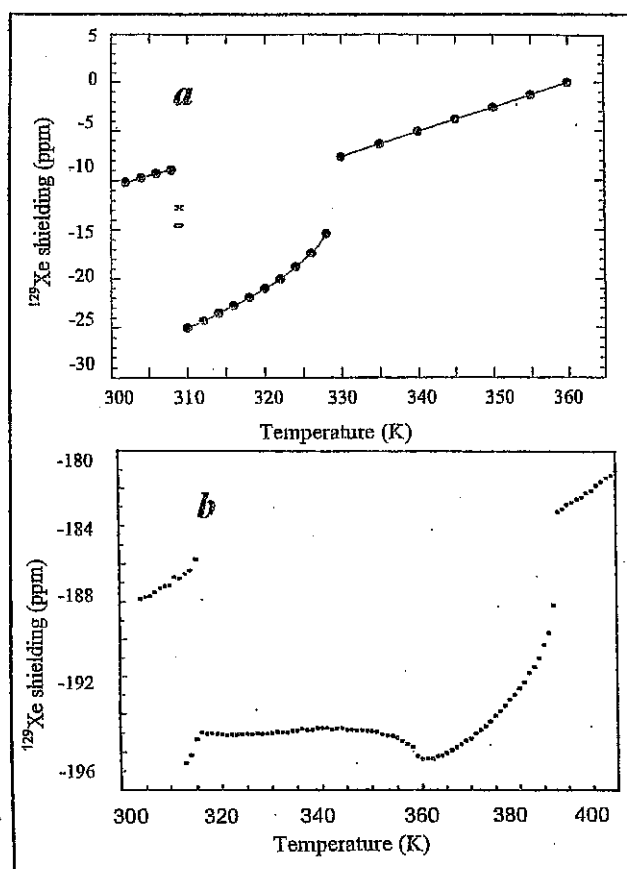


Figure 8 - ^{129}Xe shielding as a function of temperature.

(a) The LC solvent is a mixture of two LCs (ZLI1167 and EBBA) with opposite sign of diamagnetic anisotropy. At the highest temperatures the LC appears in isotropic phase. Lowering of temperature leads to transition to nematic phase where $\mathbf{n} \parallel \mathbf{B}$, and finally to smectic phase where $\mathbf{n} \perp \mathbf{B}$. The shielding value at the highest temperature is set as a reference. (b) Again at the highest temperatures the LC (NCB84) is isotropic. When lowering temperature, nematic, smectic A, smectic C and other smectic phases appear. Shielding is referenced to that of bulk gas (ca. 6 atm, 300 K).

Additional information about TLCs can be obtained by applying a theoretical model according to which the ^{129}Xe shielding can be represented in the form [49]:

$$\sigma(T) - \sigma_0 = \rho(T) \{ \sigma'_d [1 - \varepsilon(T - T_0)] (1 + 2c\gamma_1^2(T)) + \frac{2}{3} P_2(\cos\theta) \Delta\sigma'_d [1 - \Delta\varepsilon(T - T_0)] [S(T) + 2c\sigma_1(T)\gamma_1(T)] \} \quad (7)$$

where $\rho(T)$ is the LC density at temperature T , and the temperature dependence of the shielding constant and shielding anisotropy are assumed to be linear and are described by the coefficients ε and $\Delta\varepsilon$, respectively [50]. In equation (7), σ_0 is the shielding constant of the reference, T_0 the reference temperature, σ'_d and $\Delta\sigma'_d$ are the temperature-independent isotropic shielding constant and anisotropy of the shielding tensor (in ppm/g $^{-1}$ cm 3), respectively. The anisotropic part in the shielding arises from the deviation of the xenon electron cloud from spherical symmetry because of the anisotropic surroundings. The coefficient c measures the deviation of the xenon distribution from uniform distribution, and $S(T)$, $\sigma_1(T)$ and $\gamma_1(T)$ are orientational order parameters: $S(T)$ is the normal second-rank orientational order parameter, $\sigma_1(T)$ the mixed translational-orientational

order parameter, and $\gamma_1(T)$ the translational order parameter. $P_2(\cos\theta)$ is the second-order Legendre polynomial with θ being the angle between the liquid crystal director and the external magnetic field.

Least-squares fit of function (7) to experimental data allows in favorable cases (when the temperature ranges of mesophases are wide enough) the determination of the temperature dependence of all three orientational order parameters. In the smectic C phases, the derivation of the temperature dependence of the tilt angle (angle between the layer normal and director \mathbf{n}) also becomes feasible.

Another quantity, besides the ^{129}Xe shielding, that gives valuable information about phase transitions and phase structure is the self-diffusion coefficient of ^{129}Xe . The ^{129}Xe self-diffusion tensor in smectic liquid-crystalline environments appears to be remarkably anisotropic, and consequently gives information about changes in the smectic layer structure that occur between different smectic phases.

To conclude, ^{129}Xe NMR experiments on xenon dissolved in liquid crystals may be utilized in the determination of: (a) the sign of the anisotropy of diamagnetic susceptibility tensor; (b) phase transition temperatures; (c) phase structures; (d) orientational order parameters. Experiments with ^{131}Xe give additional information for the determination of the above-mentioned properties but also on the electric field gradients created by LC molecules. A review of the NMR of noble gases, including xenon, in liquid crystals can be found in [51].

^{129}Xe NMR applied to polymers

Before describing some ^{129}Xe NMR experiments on bulk polymer materials, it is worthwhile to show with a few selected examples some general aspects of ^{129}Xe NMR of polymers. The first question to address is where sorbed Xe atoms are located in a polymer material, or rather where they are not located. With a diameter of 0.44 nm, the Xe atom is clearly larger than the interchain distance for most crystalline polymers. In general this means that, when Xe atoms are found in crystalline domains, they must be in defect areas.

A clear example for the absence of Xe in crystalline polymers is shown in figure 9 for highly stretched polyethylene (PE) fibers. From X-ray experiments it is known that the crystallinity of the semicrystalline PE fibers increases with stretching. In figure 9, the NMR signal of absorbed ^{129}Xe decreases with stretching, which shows that the Xe is practically absorbed only in the amorphous domains and/or in the interface between crystalline and amorphous domains of PE. The absence of Xe in crystalline polymers also is due to the fact that the polymer chains therein are usually rigid. The energy to deform the chains so that a Xe atom can be incorporated between them is too high.

The mobility of the chains plays an important role for the line-width of the Xe resonance in amorphous polymers. Figure 10 shows the line-width of the ^{129}Xe resonance in polymethylmethacrylate (PMMA) as a function of temperature. It falls drastically when the glass transition temperature T_g is approached. The mobility of the polymer chains in amorphous domains affects the ^{129}Xe line-width while it makes it possible for the Xe atom to move rapidly from one location to another, thereby averaging out local differences in Xe chemical shift and dipolar interactions with proton spins.

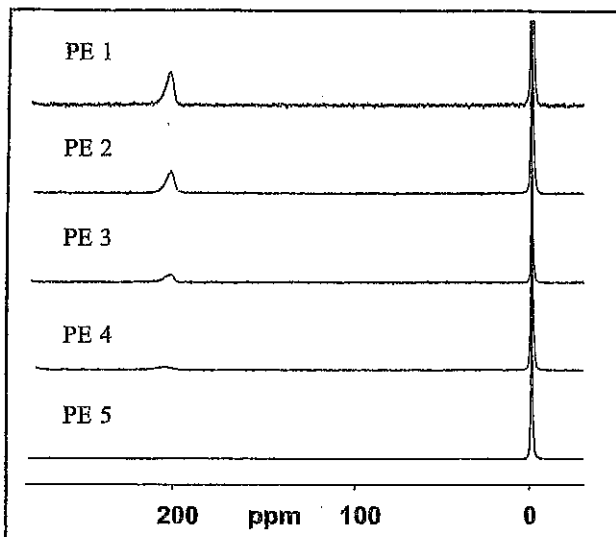


Figure 9 - The ^{129}Xe NMR spectrum of PE fibers as a function of stretching. The young modulus of the fibers increased from 38 GPa for PE1 to 131 GPa for PE5 [46].

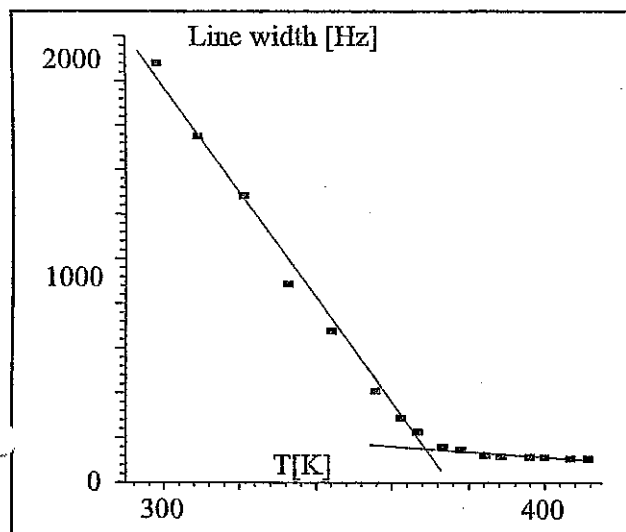


Figure 10 - The ^{129}Xe NMR line width as a function of temperature for poly(methylmethacrylate) (PMMA). The glass transition temperature of PMMA is about 375 K. The line width dependence clearly shows that the PMMA chains already start to become mobile far below T_g [42].

The chain mobility also influences the rate of Xe absorption in an amorphous polymer: it takes several weeks for PMMA at room temperature to absorb enough Xe for an NMR signal to be detected, in contrast to materials above their T_g .

From figure 10, it can be concluded that room temperature ^{129}Xe NMR spectroscopy is especially well suited for the investigation of amorphous domains in polymer materials of which the glass-transition temperature T_g is well below room temperature, as in elastomers.

^{129}Xe NMR of elastomers

Many elastomers are used as components in commercial materials, as blends, copolymers or composites. The chemical shift of ^{129}Xe dissolved in a given polymer is unique. Consequently, binary polymer blends with large domain sizes exhibit two ^{129}Xe NMR lines (in addition to the always present free Xe gas peak at 0 ppm). As an example, figure 11 shows the ^{129}Xe resonances of xenon in the amorphous domains of high density polyethylene (PE), of isotactic polypropylene (iPP) and of a blend of iPP and a PE-PP copolymer [52].

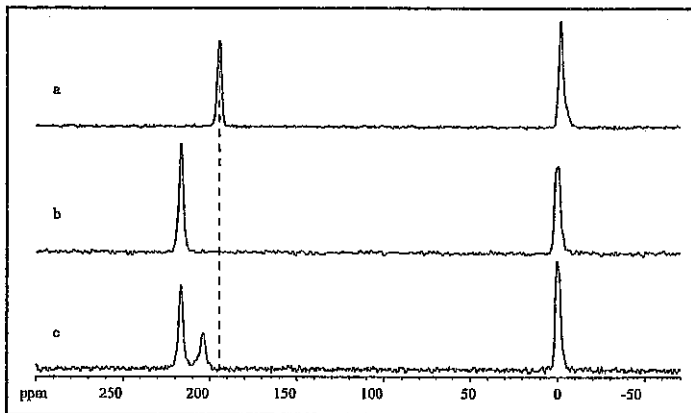


Figure 11 - The ^{129}Xe NMR spectra of (a) high-density PE, (b) iPP and (c) of a blend consisting of 80% iPP and 20% of a PE-PP copolymer.

The line positions show that the Xe absorbed in the iPP domains of the blend is identical to Xe in iPP itself, but that the Xe in the PE-PP copolymer domains has a chemical shift in between those of Xe in PE and in iPP. For Xe the PE-PP copolymer domains are homogeneous. The chemical shift of Xe in the PE-PP copolymer depends on the PE/PP composition [52].

In a model of Miller *et al.* [53] the Xe chemical shift is proportional to the difference in interaction energy between units of neighboring polymer chains with and without an enclosed xenon atom. That the chemical shift for Xe in PP is higher than in PE shows that it costs more energy to incorporate a Xe atom between PP chains than between PE units. This is in agreement with the fact that the T_g of amorphous PP (ca. 273 K) is higher than that of amorphous PE (ca. 230 K).

An important aspect of the study of ^{129}Xe NMR on polymers is the mobility of the Xe atoms. The effect of the Xe mobility on the line-width was seen in figure 10. On a longer time-scale mobility is also important. For instance, the existence of two resonances in the spectrum of the blend in figure 11c implies that the motion of the Xe atoms is not so fast that during the NMR characteristic time τ (in the spectra of figure 11 of the order of the length of the free induction decay, ms range), the Xe atoms can move between the two different domains. By changing the characteristic time of the experiment, together with knowledge about the self-diffusion coefficient D of Xe in the material, the domain sizes can be estimated from the Einstein relation: $\langle r^2 \rangle = 6D\tau$.

Two-dimensional exchange NMR experiment [54] have been performed where the characteristic time (« mixing

time ») has been lengthened to 5 s. The presence of cross-peaks indicates an exchange of Xe between the two domains within 5 s.

Self-diffusion of Xe atoms in elastomers

Pulsed field gradient echo (PFGE) NMR experiments allow the direct measurement of the Xe self-diffusion coefficient in various materials. Here we limit ourselves to systems with elastomer components. For a very similar system as shown in figure 10, a blend of PP and the ternary copolymer ethylene-propylene-norbornene (EPDM), the Xe diffusion coefficients in the PP matrix and in the EPDM domains were determined and compared to the diffusion coefficients in the pure materials (table 1) [55]. In the blend the diffusion coefficients in the PP matrix and in the EPDM domains are quite similar and lie between the values for the pure components, while during the characteristic time of the diffusion experiment (here 1.2 s) the Xe atoms exchange many times between the matrix and the EPDM domains. With the data of table 1 the average EPDM domain size for the PP/EPDM blend can then be estimated. The average size of the EPDM domains in the PP/EPDM blend is therefore clearly larger than 0.6 μm and smaller than 20 μm . By shortening the diffusion time in the PFGE experiment, the range of the average EPDM domain size could be further decreased, thereby making the method applicable for the determination of average domain sizes. The average domain size range determined here agrees with scanning electron microscope (SEM) measurements from which sizes of 1-3 μm can be estimated.

Table 1:

Xe diffusion coefficient D (cm ² /s) in PP, EPDM and in the PP/EPDM blend		
	Xe in PP	Xe in EPDM
PP	3.8×10^{-12}	
EPDM		78×10^{-12}
PP/EPDM blend	8.6×10^{-12}	12×10^{-12}

NMR of xenon gas dissolved in pure liquids and isotropic solutions

Both ^{129}Xe and ^{131}Xe NMR studies have been reported for monatomic xenon gas dissolved in pure liquids and solutions [1]. ^{131}Xe NMR studies mainly concern relaxation time measurements [56]. The magnitude of the nuclear quadrupole moment of the ^{131}Xe nucleus ($I = 3/2$) is large enough for its relaxation to be dominated by the quadrupolar mechanism without leading to excessive signal broadening. ^{131}Xe is a spin-spy suitable for the investigation of the electrostatic properties of organic solvents and other hydrophobic environments. Indeed, experimental data and computer simulations have shown that the fluctuating electric field gradients responsible for the ^{131}Xe relaxation are primarily due to the permanent electric moments of surrounding molecules. Interestingly, the ^{131}Xe relaxation rate for xenon dissolved in dipolar and various non-dipolar solvents have been found to be similar [56]. These studies highlighted the central role of permanent electric moments of higher order than the dipole

in solvent effects and lead to a revision of the notion of molecular polarity.

In pure liquids, ^{129}Xe relaxation times are hundreds of seconds long and narrow signals, line-width typically less than a few hertz are therefore observed. The very long experimental times, the presence of traces of paramagnetic impurities as well as diffusion and convection in the liquid, usually make ^{129}Xe NMR relaxation studies rather difficult to carry out, at least using thermally polarized xenon. It has been shown that in diamagnetic systems the dominant relaxation mechanism is the intermolecular nuclear magnetic dipole-dipole mechanism [57]. Polarization transfer experiments using thermally polarized ^{129}Xe and, particularly, hyperpolarized ^{129}Xe (SPINOE experiments), have definitely confirmed the importance of this mechanism [58-59]. For xenon trapped in dissolved diamagnetic cage molecules, ^{129}Xe relaxation times of the order of ten seconds have been measured and significant broadening of the signals can be assigned unambiguously to dynamic exchange processes [58, 60]. In these types of systems, the exchange between trapped xenon and xenon in the solvent is likely to be fast on the relaxation NMR time scale. In paramagnetic systems, ^{129}Xe relaxation times are considerably shortened as a consequence dipole-dipole magnetic interactions with the paramagnetic centers [61-62]. This will be discussed below for xenon dissolved in aqueous solutions of metmyoglobin.

Chemical shifts are by far the most frequently exploited parameter in xenon NMR. The chemical shift of dissolved monatomic xenon ranges over more than 250 ppm; such a huge solvent effect clearly demonstrates the sensitivity of this parameter to the xenon atom surroundings. Solvent effects on the xenon chemical shift have been shown to be directly related to the xenon-solvent dispersive interaction energy [63] and have been interpreted in terms of additive group contributions. The xenon chemical shift is highly temperature dependent. It may also significantly depend on the xenon concentration in solution as a consequence of xenon-xenon interactions. Such an effect is well known in the gas and adsorbed phases and can be exploited to determine the amount of xenon in solution.

Probing cavities by ^{129}Xe NMR

The fact that the volume of a xenon atom is comparable with the volume of internal cavities present in various organic host systems and proteins, and that it is chemically inert, makes this hydrophobic atom very suitable for the structural and dynamic study of many systems.

Studies undertaken on the complexation of xenon by organic host systems in solution, ranging from α -cyclodextrin to self-assembled host molecules [58, 60, 64-67] have shown that it is possible, using thermally polarized or HP xenon, to obtain quantitative data on these systems and on their ability to complex xenon. When xenon is in slow exchange on the xenon chemical shift time-scale, the chemical shift of xenon within the host cavity can be directly observed, and if the exchange is not infinitely slow information on the exchange dynamics can be easily obtained from line-width analysis. For xenon in fast exchange, a single resonance line is observed and the chemical shift is the weighted average of the xenon chemical shift in the various environments. The experimental data are then interpreted on the basis of a three-site model for xenon in solution, in which the xenon and the host molecule can form a 1:1 host-guest pair characterized by an equilibrium constant K , and for

which the non-complexed fraction of xenon is distributed between xenon in the close environment of the host and xenon in the bulk phase.

For example, it has been shown that the relatively apolar internal cavity of α -cyclodextrin (α -CD, figure 12a) can complex xenon [60, 67]. The equilibrium constant was determined for the xenon- α -CD system in water ($\sim 20 \text{ M}^{-1}$ at 298 K) and in DMSO ($\sim 2 \text{ M}^{-1}$ at 298 K). The larger constant measured in water is a clear indication that hydrophobicity plays a major role in complex formation. The chemical shift of xenon included in the α -CD cavity was found to be independent of the solvent and in excellent agreement with the value measured in the solid state [68]. The xenon- α -CD system is the first for which selective enhancements of ^1H NMR signals were observed using laser-polarized xenon [59].

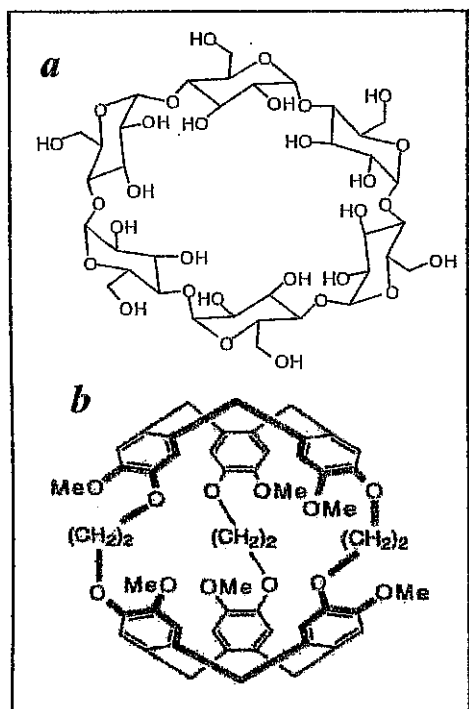


Figure 12 - Structures of (a) α -cyclodextrin and (b) cryptophane-A.

A system which has proven to be of great interest is the chiral cryptophane A host (CA, figure 12b). The xenon-CA complex is the most stable xenon-host complex reported to date ($K > 3000 \text{ M}^{-1}$ at 278 K) [64]. The fact that the xenon atom fits the cavity without restraining the dynamics of the cage contributes to this high stability. The complexation kinetics is slow on the ^{129}Xe chemical shift time-scale. Interestingly, unexpected xenon concentration dependences of the line-widths were observed and the correlated escape and inclusion of xenon was identified as the prevailing exchange mechanism. The xenon-CA system has been the object of much investigation especially using hyperpolarized xenon [58, 69] and is being developed as a NMR-based xenon biosensor (see below).

Mislow and Siegel defined many years ago as « *chirotopic any point or segment of the molecular model, whether occupied by an atomic nucleus or not, that resides within a chiral environment* ». With xenon NMR it has been

shown experimentally that the CA cavity is chirotopic and that monatomic xenon is chiralized when it is in this chiral environment [70]. The ^{129}Xe NMR spectra at 278 K in a racemic solution of CA containing xenon and increasing amounts of a chiral chemical shift reagent are reported in figure 13. The chemical shift of the included xenon is identical for the two enantiomers of CA dissolved in the absence of the chemical shift reagent. In its presence two ^{129}Xe resonance lines are observed. It can therefore be argued that the xenon atom in the CA cavity is chirotopic, and that it becomes diastereotopic as soon as the chiral host CA is put in the presence of a chiral partner. These results are the first example of the chiralization of a spherical and neutral atom.

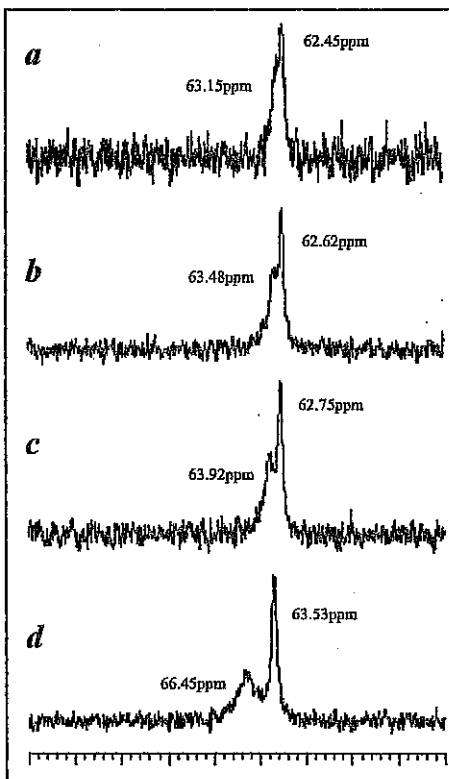


Figure 13 - ^{129}Xe NMR spectrum of xenon dissolved in a racemic solution of the two enantiomers of cryptophane-A (CA) in $\text{C}_2\text{D}_2\text{Cl}_4$ at 278 K in the presence of increasing amounts of a chiral europium chemical shift reagent (CSR): (a) $[\text{CSR}]/[\text{CA}] = 0.08$; (b) $[\text{CSR}]/[\text{CA}] = 0.16$; (c) $[\text{CSR}]/[\text{CA}] = 0.24$; (d) $[\text{CSR}]/[\text{CA}] = 0.52$.

^{129}Xe NMR has also proved to be a powerful method for investigating hydrophobic cavities in proteins and protein surfaces [71-74]. X-Ray studies have shown that xenon binds reversibly to specific hydrophobic cavities in proteins [75]. Metmyoglobin (MMb) was the first protein to be shown by X-ray crystallography to bind xenon reversibly in its proximal cavity next to the heme group, and also the first one to be studied by xenon NMR [72]. This system, for which xenon is in fast exchange between all possible environments, has been further characterized by several groups using both thermally and HP xenon. The analysis of xenon chemical shifts in the presence of proteins which do not have specific xenon binding sites, suggest that non-specific interactions exist between xenon and the protein exteriors and the data can be analyzed in term of parameters which characterize the protein surfaces [73-74].

As mentioned previously, relatively few studies have been published on the measurement of ^{129}Xe longitudinal relaxation times. The ^{129}Xe longitudinal relaxation rate in MMb solution is, however, dominated by the paramagnetic contribution due to the interaction of the xenon atom in the proximal cavity and the high-spin Fe^{3+} of the heme group. Consequently ^{129}Xe longitudinal relaxation times are shortened and their measurement is feasible. The ^{129}Xe longitudinal relaxation rates of the complexed and the uncomplexed xenon have been determined, and non-specific interactions with the protein surface have been further characterized [59]. The relaxation study of xenon atoms trapped in protein cavities close to a paramagnetic ion could therefore be an efficient method to determine the xenon-ion distance and consequently the position of the cavity with respect to the paramagnetic center.

Molecular palpation by ^{129}Xe NMR

Most recently, ^{129}Xe NMR has been used to study systems in solution that do not complex xenon in a specific site but are involved in a configurational or a conformational equilibrium. ^{129}Xe NMR has, for example, been used to monitor the mutarotation of D-glucose in aqueous solutions [76]. The two anomers of D-glucose are diastereoisomers that only differ by the configuration at one of their six stereogenic centers. Once the α or β anomer of D-glucose is dissolved in a solvent, epimerization occurs and the concentration of both anomers changes until equilibrium is reached. The process was monitored by measuring, as a function of time, the ^{129}Xe chemical shift in solutions containing initially one or other of the pure anomers (figure 14). The results show that the xenon methodology can indeed be used to study the equilibrium between two molecules that are structurally nearly identical. The thermodynamic and kinetic constant characteristics of the system were determined and an H/D isotopic effect was also observed.

The ^{129}Xe NMR methodology has been also used to study the conformational equilibrium of cyclohexanol [77].

For mono-substituted cyclohexanes, the activation energy for the chair-chair equilibrium is such that at room temperature it is impossible to isolate the conformers and determine their specific properties. The classical NMR methodologies used to study the conformational equilibrium of mono-substituted cyclohexane molecules at room temperature focuses on a carbon or proton atom belonging to the molecule under investigation. The xenon atom was used as an external spy to monitor the equilibrium. The results show that xenon is indeed sensitive to the interconversion equilibrium between the axial and the equatorial isomers of cyclohexanol. The conformational equilibrium constant has been estimated and its value is in excellent agreement with the values obtained by ^1H and ^{13}C NMR.

These results show that it is possible, using ^{129}Xe NMR spectroscopy, to investigate a chemical equilibrium *via* intermolecular interactions without perturbing it. The xenon methodology can be defined as a « palpation methodology ».

In situ HP ^{129}Xe NMR of combustion

Because of the difficulties for conventional NMR with the conditions present in high-temperature gas phases, the first *in situ* NMR of combustion utilizes (HP) ^{129}Xe as a probe [8]. The chemical inertness of xenon and its temperature-dependent chemical shift within porous media provide additional advantages for HP ^{129}Xe NMR as a probe for combustion and other high temperature reactions. Furthermore, radio-frequency can readily penetrate many optically non-transparent systems that are difficult to access by measurements in the UV, visible or infrared regimes. *In situ* NMR measurements are therefore of particular interest for combustion processes that occur within opaque media. Examples are the reaction zones of smoldering processes or catalytic combustion within reactors. Previously, ultrasonic tomographic imaging has been employed for studies of smoldering processes in opaque media [78]. This technique is limited to the solid phase and can be used to study the propagation of a smoldering front. However, gas transport, flow velocities, diffusion phenomena and gas-phase reactions are only accessible to HP ^{129}Xe NMR and MRI.

The reported *in situ* NMR of combustion [8] served largely as a proof of concept work. It was demonstrated that despite the presence of paramagnetic oxygen and radicals, the xenon relaxation times are sufficiently long for gas exchange studies. The observed scale of the gas dynamics was sufficiently slow to provide hope for chemical-shift-selective spatial imaging in future work. HP ^{129}Xe was mixed with methane, and air as an oxidant was added shortly before the combustion zone within the superconducting magnet.

A photograph of the actual combustion zone is depicted in figure 15a. The gas mixture was flowed through an area with molecular sieve pellets (NaX) and ignited above the pellets. Figure 15b [78] shows one of the resulting ^{129}Xe NMR spectra taken during combustion (solid red line) in comparison with the spectrum of the same initial mixture without combustion at ambient temperature (dashed blue line). In addition to the pure gas (-0.26 ppm), a peak at -3 ppm is only observed during combustion in the presence of the zeolite. It was demonstrated by 2D-EXSY data (figure 16) that this 350 Hz-broad signal at -3 ppm originates from a region just above the bulk of the zeolite. This effect will need

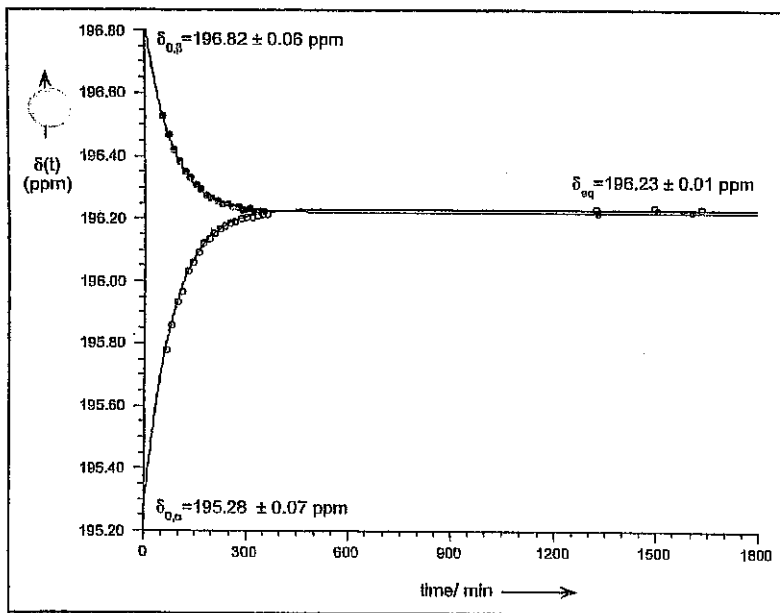


Figure 14 - ^{129}Xe chemical shift variation in 1M α -D-glucose (o) and β -D-glucose (●) solutions in D_2O as a function of time.

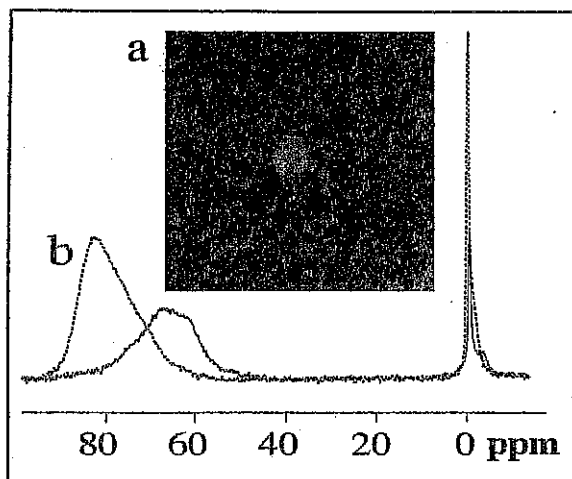


Figure 15 - Photography of the detection region of the NMR probe with radio frequency coil.

A methane-air mixture was ignited above zeolite pellets. The mixture also contained xenon for NMR detection. ^{129}Xe NMR spectra with 30% xenon (from high-density xenon optical pumping) in 70% methane is depicted. The spectrum in the absence of combustion is shown in a blue dashed line and the spectrum during combustion in a red solid line.

further investigation since neither experimental nor theoretical xenon chemical shift data are presently available for temperatures above 1000 K.

The NMR peak originating from xenon within the zeolites was strongly affected by temperature. The xenon inside the nanoporous zeolite pellets led to a signal at approximately 82 ppm at room temperature, but shifted to about 65 ppm after ignition. The shift was due to the reduced xenon loading of the porous material caused by a temperature increase within the material in the pre-combustion region through thermal conductivity and IR radiation.

2D HP ^{129}Xe NMR exchange spectroscopy (EXSY) was applied to study xenon transfer between the nanoporous material and the combustion zone. The peaks in EXSY experiments are a function of two correlated chemical shift values. The horizontal axis in figure 16 relates to the chemical shift of the xenon at the beginning of the experiment ($t = 0$), while the vertical axis describes the chemical shift after a time period $t = \tau$ has passed. The signals will appear on the diagonal when the chemical shift values on the horizontal and vertical axes are identical. No cross-peaks appear in figure 16a proving that no exchange between the various regions occurred during short exchange times $\tau \leq 5$ ms. The corresponding 1-D spectrum is displayed above the EXSY for clarity. The appearance of cross-peaks in the 2D spectra at longer τ times is caused by gas transport between the different regions. The location and intensity of the cross-peaks indicate the exchange direction and the amount of material that is transported during

the delay time. Since combustion is a non-equilibrium process and gas transport is directional, the cross-peaks in the EXSY spectra for larger exchange times τ are seen to be asymmetric in figure 16.

At $\tau = 20$ ms, a single cross-peak appeared because of the exchange between xenon located in the nanoporous material and the -3 ppm gas phase. The EXSY proved that transfer of xenon from the zeolite did not take place to the -0.26 ppm region at $\tau = 20$ ms. However, figure 16b shows also a (barely resolved) cross-peak that demonstrated exchange from the -3 ppm to the -0.26 ppm region. Due to the gas flow direction, it was concluded that the -3 ppm zone was located between the porous material and the bulk of the flame region further above. For longer τ times (figure 16c-d), an exchange cross-peak directly between the material phase and the gas phase at -0.26 ppm appears. The diagonal peaks of the combustion region disappear because the gas is transported out of the detection region after long delay times and no more signal can be detected after $t = \tau$ for the gas phase. It seems that Xe NMR is the only way today to study the exchanges of gas in such heterogeneous system.

Improvement of Xe NMR technique

The ability to hyperpolarize xenon nuclear spins through spin exchange optical pumping [5] opens new experimental possibilities to study surfaces or targets at very low

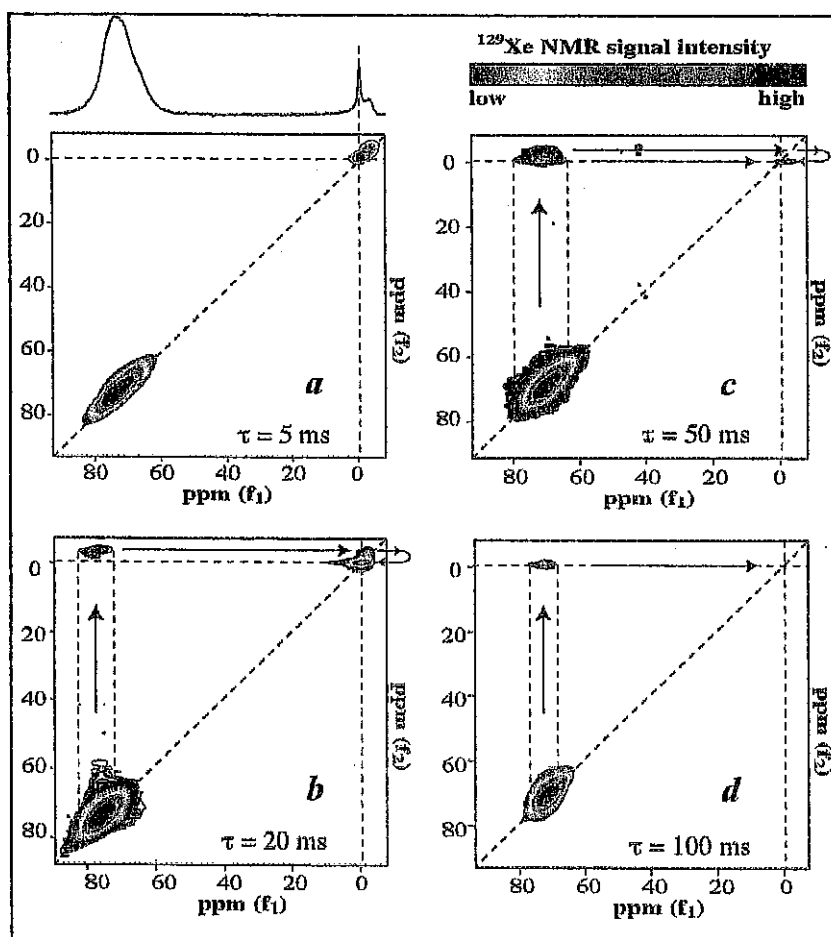


Figure 16 - ^{129}Xe 2D EXSY NMR spectra recorded during combustion for various exchange times.

concentration, image void spaces, or study gas flow. However, even this enhanced sensitivity may not be sufficient if the sample has a very low porosity or if the target molecule is only available at low concentration. Furthermore, the specificity of xenon is low if the sample is a complex mixture of different potential targets. We present two techniques that can help to overcome these problems. To enhance the selectivity of xenon NMR, the xenon atom can be functionalized with a protein cavity or a cryptophane cage that matches the size of xenon. Molecules with known selectivity for a specific biomolecular target can be modified by introducing a xenon-binding cavity or by attaching a cryptophane cage. Cage-associated xenon has a unique chemical shift separate from the solution chemical shift, unlike xenon bound to a protein cavity. Therefore the sensitivity for specific analytes is enhanced considerably by using a cryptophane cage. Another approach to improve sensitivity is remote detection, which is based on the fact that encoding and detection of information in NMR often have different requirements. Spatially separating encoding and detection enables us to separately optimize both steps.

Remote detection

Remote detection is a methodology allowing for the separate optimization of encoding and detection steps in an NMR experiment [79]. In conventional NMR both of these take place in one coil inside a homogeneous magnetic field. A series of radio-frequency (rf) pulses are delivered to the sample to encode the nuclei with structural information, such as their local environment or connectivity. In the case of imaging, spatial information may be encoded by using magnetic field gradients in addition to the rf pulses. In the remote detection mode, the encoded information is stored as magnetization of ^{129}Xe , which can be detected later under optimized conditions. The signal is thus read out point-by-point rather than in a single shot. Performing NMR in this way adds a dimension to the experiment but provides a flexibility not permitted by conventional NMR, namely, the ability to tailor the encoding environment to the requirements of the sample in shape, size, and field strength without compromising the quality of the signal. The detector is optimized independently, which not only allows encoding and detection at different field strengths, but it also facilitates the use of different kinds of detectors.

The remote detection modality requires the use of a sensor to survey the environment of interest and to report the encoded information. In principle, this can be achieved with any NMR-active nucleus provided it has a longitudinal relaxation time, T_1 , which is longer than the travel time of the sensor medium from the encoding to the detection site. Xenon is chosen as « signal-carrier » because of its long T_1 , its sensitivity to the chemical environment, its chemical inertness, and the high polarization attainable through spin-exchange optical pumping. Xenon is therefore a good transport medium capable of gathering chemically rich information about its environment and retaining this information for a sufficiently long time to allow transport out of the sample to the detector.

With remote detection there are a variety of different detection methods available (figure 17). Examples of sensitive detectors are optimized Faraday coils, magneto-meters like Superconducting Quantum Interference Devices (SQUID) [80], or atomic magnetometers [81] and spin-exchange optical detection [82]. In proof-of-principle experiments,

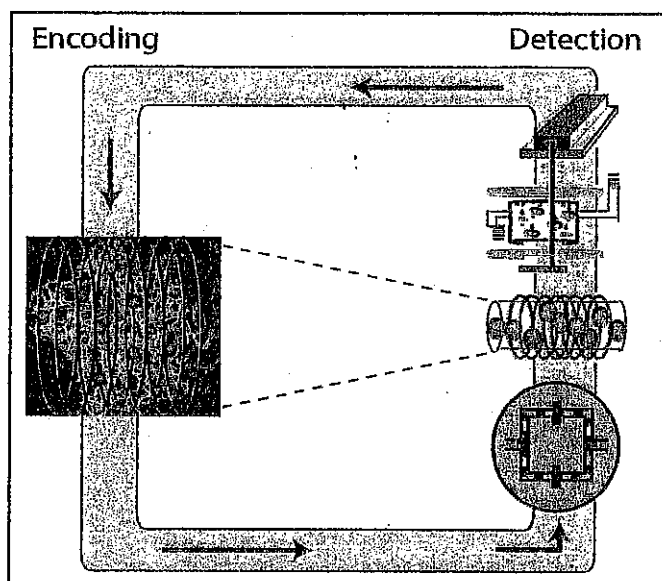


Figure 17 - Remote detection schematic.

Laser polarized ^{129}Xe is prepared by spin exchange optical pumping to achieve polarizations on the order of 1-10%. The gas is transferred from the polarization cell and allowed to infuse the sample matrix where it is encoded by a large coil with a poor number of spins per volume ratio. The sensor is then removed from the sample and detected under optimized conditions. The encoded information can be read out using a more sensitive rf-coil or by alternative detection methods such as SQUIDS or optical detection.

some of us used small, sensitive Faraday coils for detection. In detecting the chemical shift of xenon in an aerogel, a signal-to-noise improvement of 10 was achieved by remote reconstruction. This was primarily attributed to the increase in the number of nuclei per volume that was achieved when the coil did not need to accommodate the aerogel sample [79].

In addition to chemical shifts, imaging information of void space can be reconstructed remotely [83]. A 13 mm phantom inscribed with the letters, CAL was imaged at 7 T. The images (figure 18) highlight the signal enhancement possible using remote detection. The fully reconstructed image is the sum of ten batches of gas which reach the detector at different times due to their distance from the detector and represents an enhancement of approximately 1.7 times that of the directly detected image.

A promising application of remote detection is using it to amplify the signal of xenon in biomolecular solutions. The following section will briefly highlight the use of ^{129}Xe for biomolecular assays; interested readers are referred to a more thorough review of this topic presented elsewhere [84].

Xenon biosensor

The ^{129}Xe NMR has several unique advantages as a biomolecular probe. These include the ability to probe opaque environments, the potential for multiplexing, and the absence of xenon from biomolecules provides zero background signal. When in an aqueous protein solution, xenon is in fast exchange between all available sites, and the observed xenon chemical shift is an average of the chemical shift at each site weighted by its binding affinity [74, 85]. These sites include bulk solvent, protein surfaces and protein cavities. Some protein cavities bind xenon with moderate affinity ($\sim 100 \text{ M}^{-1}$) and therefore significantly contribute to the observed xenon chemical shift [86]. Protein conformational changes that alter

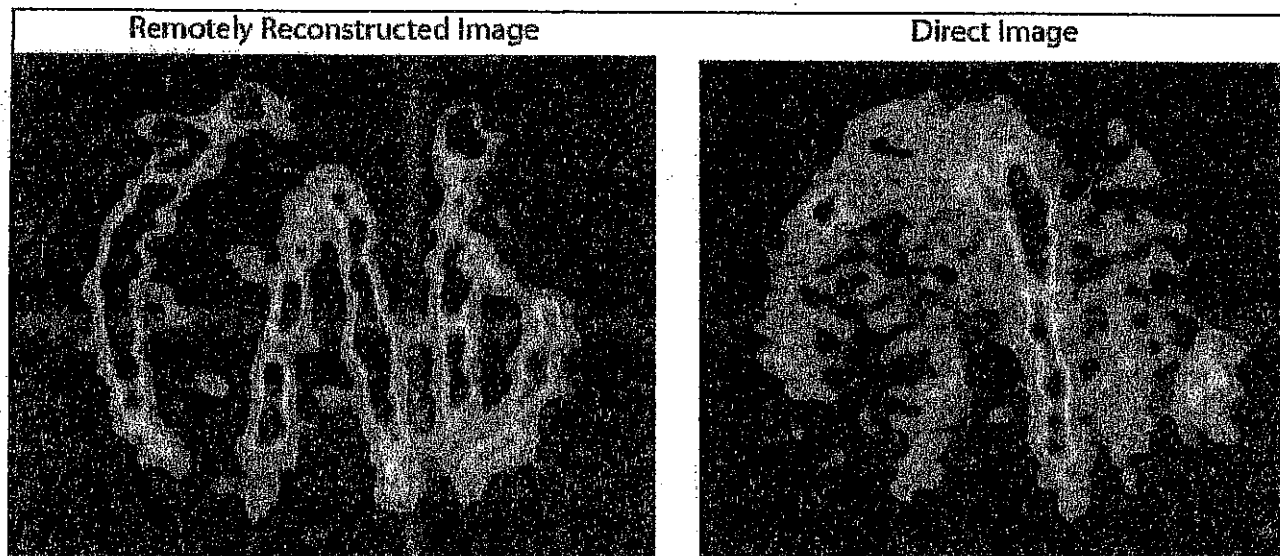


Figure 18 - ^{129}Xe remotely detected void space image.

A 13 mm phantom inscribed with the letters CAL was imaged. The remotely reconstructed image is the result of several batches of gas reaching the detector at varying times based on flow path. The image has an enhancement of 1.7 times that of the directly detected image.

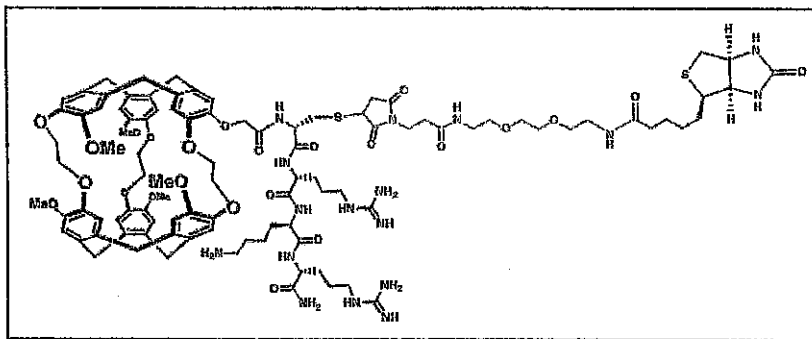


Figure 19 - The original xenon biosensor consists of a xenon-binding cryptophane-A supramolecular cage (black), a solubilizing peptide (blue), a linker (green), and a biotin ligand (red).

A protein cavity's xenon shift or binding affinity can be detected by monitoring the xenon solution chemical shift. The maltose binding protein (MBP) was the first example of a protein whose conformational state could be monitored with ^{129}Xe NMR [85-86]. Since then, ^{129}Xe NMR has been used to detect more subtle protein conformational changes in the *E. coli* chemotaxis Y protein [84]. This method has been greatly extended by demonstrating the ability to engineer a conformation-sensitive xenon-binding cavity into a protein that does not naturally possess one, the ribose-binding protein [87].

Greater sensitivity and experimental flexibility are possible by separating the xenon analyte peak from the xenon solution peak. To accomplish this, a « functionalized » xenon biosensor has been developed [88]. The xenon biosensor consists of a xenon-binding supramolecular cryptophane-A cage (figure 12) ($K_a > 1000 \text{ M}^{-1}$) tethered to a water-solubilizing peptide and biotin ligand (figure 19). Unlike for protein cavities, xenon is in the limit of slow exchange between the cryptophane-A cage and bulk solution, resulting in a single resonance for the encapsulated xenon that is well resolved from the xenon solution peak (figure 20). This allows changes in the biosensor-bound xenon to be directly observed, lead-

ing to improved sensitivity of analyte-associated xenon. The unique exchange properties of the xenon biosensor enable even greater sensitivity enhancement by two new techniques called exchange signal averaging and indirect assay; interested readers are referred to the original text for a complete description [88]. When avidin binds to the biotinylated biosensor, the chemical shift of the encapsulated xenon moves downfield and broadens (figure 20), reporting the presence of avidin. Likely causes of the shift and broadening of xenon biosensor upon binding include structural deformation of the

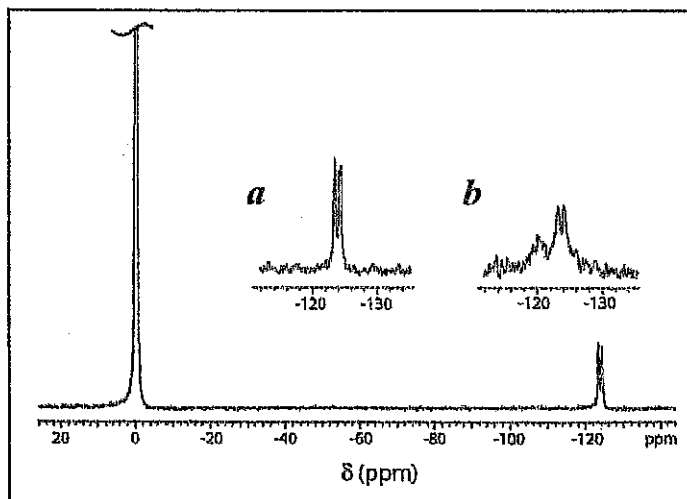


Figure 20 - ^{129}Xe NMR spectra monitoring the presence of avidin.

The main figure shows the spectrum of xenon biosensor in the absence of avidin. The peak at -124 ppm corresponds to encapsulated xenon referenced to the chemical shift of xenon in water. The inset shows the xenon biosensor resonance before (a) and after (b) the addition of one half equivalent of avidin. In the presence of avidin a new, broad resonance appears -2 ppm downfield [90].

cage, changes in the cage's vibrational and rotational movements, and increased biosensor correlation time [88]. The extraordinary sensitivity of encapsulated xenon to small changes is also exhibited when the molecular structure of the cryptophane cage or attached chemical moiety is altered. For example, lengthening the bridges between the caps by one methylene group changes the chemical shift of cryptophane-encapsulated xenon by ~30 ppm, and altering the number of attached chiral centers changes both the chemical shift and number of xenon biosensor resonances [88]. The strong dependence of encapsulated xenon on biosensor structure indicates that the chemical shift of xenon biosensors can be tuned to create many unique xenon biosensors with different chemical shifts. Each unique xenon biosensor could then be functionalized to target a different analyte, allowing for parallel detection of several analytes simultaneously [88].

Hyperpolarized ^{129}Xe : a potential biological tracer for *in vivo* NMR spectroscopy and imaging

HP ^{129}Xe NMR characteristics relevant to *in vivo* use

Due to the non-renewable HP magnetization, the ^{129}Xe NMR signal always decreases. The system tends to recover its thermal equilibrium through different processes following the longitudinal relaxation rate T_1 . For example, T_1 decreases in the presence of paramagnetic molecules (e.g. O_2 *in vivo*) or when xenon flows across magnetic field gradients. In particular, it decreases markedly in blood and tissues in a few seconds. Due to this shortening of T_1 after administration *in vivo*, the use of HP gas is more problematic in living beings. Two routes of administration are suitable: injection, after dissolving in an appropriate liquid carrier agent, or inhalation. In this respect, brain tissue perfusion and lung ventilation [89] are the principal targets that were studied essentially in animals in the former case.

Brain perfusion and corresponding *in vivo* imaging

Blood supplies biological tissues with nutrients, oxygen... necessary for their normal working. It is also part of many regulatory processes and removes wastes as well as carbon dioxide. Blood flow is usually expressed as a flow per unit of mass of the tissue of interest (mL/min/100 g of tissue). The cerebral blood flow (CBF) is of particular importance as brain has low storage capability but rapid and large requirements due to its metabolic activity. Moreover, the CBF is altered relative to normal values in many pathological conditions: head injury, epilepsy, stroke, neurodegenerative diseases... [on a global (gCBF) or regional (rCBF) scale]. These variations

are either sources or consequences of brain tissue damage. Although of importance, quantifying CBF (necessarily *in vivo*) is quite difficult, and especially imaging CBF which reflects regional variations (rCBF) is still a challenging task. A wide range of methods, using nearly all physical properties involved in medical imaging, has already been proposed. No one is, at this time, completely satisfactory due to drawbacks ranging from theoretical to practical considerations. However, among all these methods, those using xenon remain the best, stating that the rate of uptake and clearance of an inert diffusible gas by a tissue is proportional to blood flow (figure 21). In particular, scintigraphic measurement based on ^{133}Xe , a gamma emitter, is still nowadays regarded as a gold standard despite its limited resolution and low availability. Stable xenon-enhanced X-ray computer tomography (Xenon-CT) is another method clinically used. With the advent of HP ^{129}Xe , allowing NMR detection of xenon in living beings, it has been proposed to use ^{129}Xe to measure CBF using MRI techniques. We report here an example.

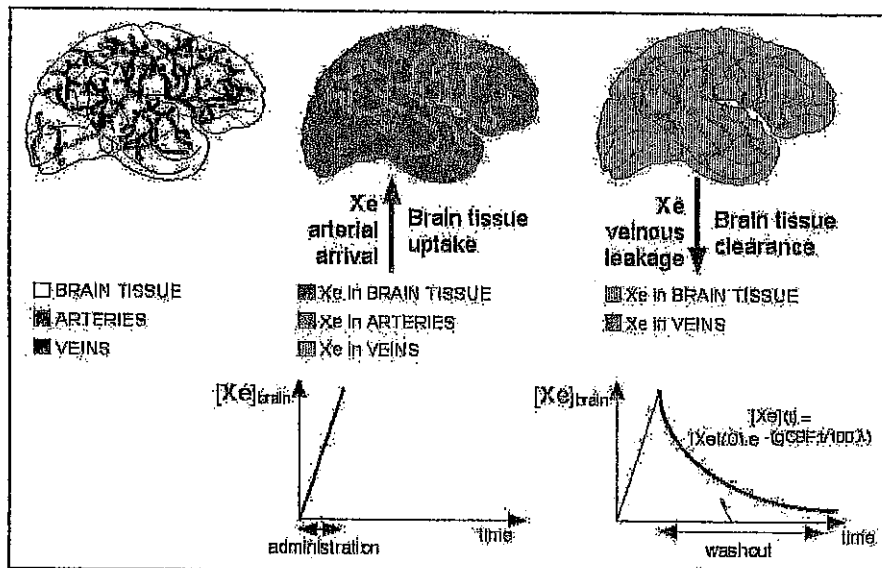


Figure 21 - Principle of CBF measurement.

$[\text{Xe}]_{\text{brain}}$ is the concentration of Xe in brain tissue, gCBF the global cerebral blood flow, t the time and λ the partition coefficient of Xe between blood and tissue.

Cerebral blood flow imaging and measurements in rat brain using HP Xe

After its preparation according to [90], the HP Xe is mixed with a lipid emulsion leading to a so-called magnetic tracer. For administration, the injection route, at first glance more invasive, combines two advantages: an appropriate carrier agent allows high dissolution of xenon while preserving its HP state; an intracarotid injection gets you as close as possible to the target organ.

For example, a 0.3-mm-i.d. indwelling catheter is inserted under general anaesthesia into the internal carotid artery after ligation of the external and common carotid arteries of Sprague-Dawley rats weighing 250-350 g. About 1-1.5 mL of the magnetic tracer, at room temperature, are manually injected at a rate of approximately 2-3 mL per minute.

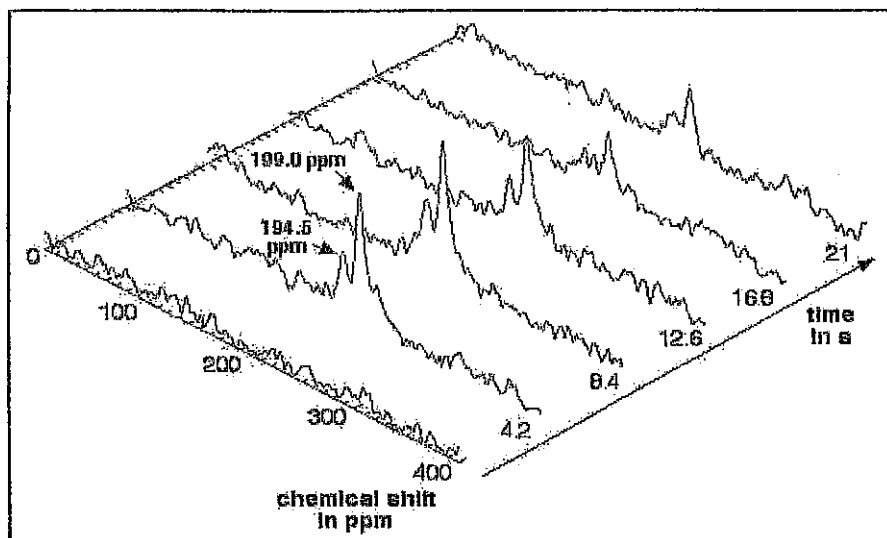


Figure 22 - Typical time-courses of the spectra of ^{129}Xe in the brain of a living rat. Only 5 of 200 phase spectra are shown (time between 2 spectra 4.2 s).

Figure 22 shows a typical spectrum obtained in the brain *in vivo* 4.2 s after magnetic tracer administration: two peaks are observed at about 200 ppm from the gas peak. The peak at 199.0 ppm is assigned to the xenon in brain tissue and that at 194.5 ppm to ^{129}Xe in lipid, in the blood vessels. Temporal evolution of the peaks can be followed as long as a signal is detectable. Raw data (area of the 199 ppm peak) are corrected for T_1 relaxation (taking a mean T_1 value from literature data) and RF pulse (taking the flip angle value) effects. The fit of the corrected data allows for global CBF calculation (mean value $160 \pm 30 \text{ mL } 100 \text{ g} \cdot \text{min}^{-1}$, in the range of the standard value accepted for rats). Furthermore, a projection-reconstruction imaging sequence leads to images of the distribution of ^{129}Xe inside the brain (figure 23). Signal hyperintensity is observed in the hemisphere corresponding to the side of injection, due to the injection conditions.

Alteration of CO_2 arterial partial pressure (PaCO_2) in five mechanically ventilated rats shows a variation of the CBF

measured in concordance with physiology: a lower value of PaCO_2 than standard causes a reduction in CBF and vice versa (figure 24).

An ideal method for CBF measurement should have several properties: giving quantitative results, with high spatial resolution, allowing continuous measurements, without modifying normal brain function, with minimal risk to patient, cost-effectiveness and clinical applicability. HP ^{129}Xe is far from satisfying all the desiderata, like any other technique currently in use. gCBF can be assessed validating the choice of the intracarotid route. Images obtained are of high spatial resolution, thanks to MRI capabilities. Generation of rCBF maps is not straightforward due to T_1 and flip angle effects, but the PaCO_2 reactive test testifies to correlation between values measured and CBF.

General conclusion

Since the first publications on Xe NMR of adsorbed xenon used a probe, this technique has shown its interest in many applications.

It is at present the only technique which is really effective for the characterization of microporous solids (e.g. zeolites) and their defects. The porosity of mesoporous solids is relatively well defined by means of nitrogen adsorption-desorption techniques. Xe NMR is however an excellent complement, in particular to demonstrate the roughness of the pore surface or, more recently, to study systems with a zeolite monolayer on the surface. It is also useful for defining the distribution of supported metals or phases adsorbed on porous solids.

This wide field of applications has been considerably extended by the advent of xenon hyperpolarization which increases the sensitivity of NMR detection by 3 or 4 orders of magnitude. This technique should be used increasingly

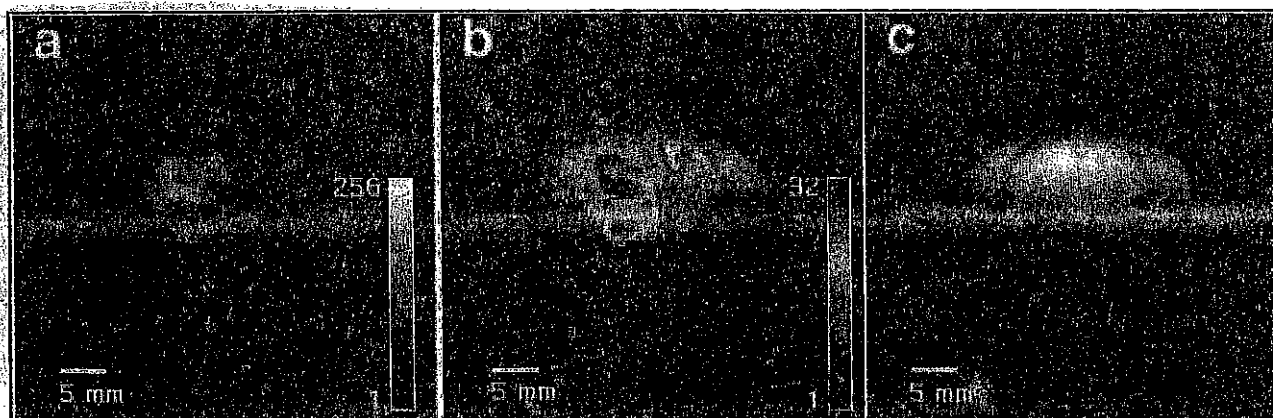


Figure 23 - ^{129}Xe (a) and corresponding ^1H (c) transverse images of rat brain. Injection was performed through the right internal carotid artery. In (b), the ^{129}Xe image was encoded to 32 false colors (with SNR threshold set to 3:1) and overlaid on the corresponding ^1H image.

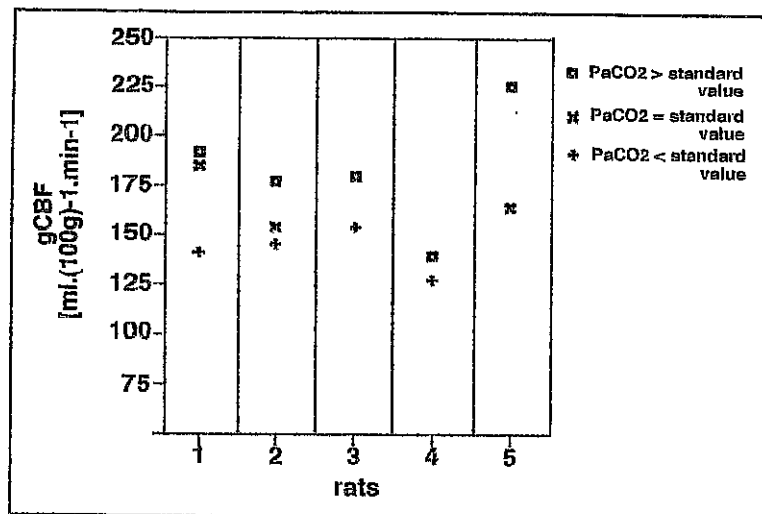


Figure 24 - Value of gCBF in five animals with different PaCO₂ values.

for the study of:

- carbon nanotubes (whose industrial importance is growing);
- solid polymers, particularly to characterize the amorphous zones and to check the homogeneity of composites;
- liquid crystals (for example: phase structures and phase transition, order parameters, etc.);
- liquid media, to define the interactions between various species, for example between proteins and their media.

Finally, although there are not yet many applications, one can be optimistic about the use of Xe NMR in the study of gas exchanges in flames.

The spectroscopic properties of ¹²⁹Xe represent a rich source of information *in vivo*: the wide chemical shift range and the precise relationship between a peak and the microscopic location of ¹²⁹Xe provide a potential tool for studying interaction at a molecular level. HP ¹²⁹Xe has not yet revealed all its potentialities in studying living tissues and requires further investigation.

References

- [1] Reisse J., Monoatomic Xenon: Its great interest in chemistry as a probe of intermolecular interactions, and its (easy) study by NMR, *New J. Chem.*, 1986, 10(12), p. 665.
- [2] Raftery D., Chmelka B.F., Xenon NMR spectroscopy, *NMR Basic Principles and Progress*, B. Blümich (ed), Springer-Verlag, Berlin, Heidelberg, 1994, 30, p. 111.
- [3] Ratcliffe C.I., Xenon NMR, *Annu. Rep. NMR Spectr.*, 1998, 36, p. 124.
- [4] Bonardet J.L., Fraissard J., Gedeon A., Springuel-Huet M.A., Nuclear magnetic resonance of physisorbed Xe-129 used as a probe to investigate porous solids, *Catal. Rev. Sci. Eng.*, 1999, 41(2), p. 115.
- [5] a) Grover B.C., Noble-gas NMR detection through noble-gas-Rubidium hyperfine contact interaction, *Phys. Rev. Lett.*, 1978, 40, p. 391; b) Happer W., Miron E., Schaefer S., Schreiber D., van Wingen W.A., Zeng X., Polarization of the nuclear spins of noble-gas atoms by spin exchange with optically pumped alkali-metal atoms, *Phys. Rev. A*, 1984, 29, p. 3092.
- [6] Driehuis B., Cates G.D., Miron E., Sauer K., Walter D.K., Happer W., High-volume production of laser-polarized Xe-129, *Appl. Phys. Lett.*, 1996, 69, p. 1668.
- [7] Moudrakovski I.L., Tersikh V.V., Ratcliffe C.I., Ripmeester J.A., Wang L.Q., Shin Y., Exarhos G.J., A ¹²⁹Xe NMR study of functionalized ordered mesoporous silica, *Journ. of Phys. Chem. B*, 2002, 106(23), p. 5938.
- [8] Aneta S., Pavlovskaya G.E., Pichumani P., Dieken T.J., Olsen M.D., Meersmann T., In situ NMR spectroscopy of combustion, *JACS*, 2003, 125(43), p. 13298.

- [9] Kaiser L.G., Meersmann T., Logan J.W., Pines A., Visualization of gas flow and diffusion in porous media, *Proceedings of the National Academy of Sciences of the United States of America*, 2000, 97(6), p. 2414.
- [10] Flabo J., Zeolite chemistry and catalysis, *ACS Monograph*, 1976, 171.
- [11] a) Fraissard J., Ito T., ¹²⁹Xe-NMR study of adsorbed xenon: a new method for studying zeolites and metal-zeolites, *Zeolites*, 1988, p. 350 and references therein; b) Springuel-Huet M.A., Bonardet J.L., Fraissard J., ¹²⁹Xe-NMR of physisorbed xenon used as a probe for the study of microporous solids, *Appl. Magn. Reson.*, 1995, 8, p. 427.
- [12] Demarquay J., Fraissard J., ¹²⁹Xe NMR of xenon adsorbed on zeolites: relationship between the chemical shift and the void space, *Chem. Phys. Lett.*, 1987, 136, p. 314.
- [13] Springuel-Huet M.A., Demarquay J., Ito T., Fraissard J., ¹²⁹Xe-NMR of xenon adsorbed on zeolites: determination of the void space from the chemical shift, *Stud. Surf. Sci. Catal.*, 1988, 37, p. 183.
- [14] Derouane E.G., André J.M., Lucas A.A., A simple van der Waals model for molecule-curved surface interactions in molecular-sized microporous solids, *Chem. Phys. Lett.*, 1987, 137, p. 336.
- [15] Ripmeester J.A., Ratcliffe C.I., Application of xenon-129 NMR to the study of microporous solids, *J. Phys. Chem.*, 1990, 94, p. 7652.
- [16] Chen Q., Springuel-Huet M.A., Fraissard J., ¹²⁹Xe-NMR of adsorbed xenon for the determination of void spaces: influence of temperature, extraframework species, amorphous phase, etc., *Stud. Surf. Sci. Catal.*, 1991, 65, p. 219.
- [17] Benslama R., Fraissard J., Albizane A., Fajula F., Figueras F., An example of the technique of studying adsorbed xenon by ¹²⁹Xe-NMR: approximate determination of the internal void space of zeolite beta, *Zeolites*, 1988, 8, p. 196.
- [18] Moudrakovski I.L., Ratcliffe C.I., Ripmeester J., Application of ¹²⁹Xe 2D-EXSY NMR to intra- and interparticle exchange in zeolites, *Appl. Magn. Reson.*, 1995, 8, p. 385.
- [19] Smith M.L., Corbin D.R., Dybowski C., Effects of temperature on xenon-129 NMR spectroscopy of xenon in zeolite rho, *J. Phys. Chem.*, 1993, 97, p. 9045.
- [20] Millot Y., Man P., M.A. Springuel-Huet, Fraissard J., Quantification of electric field gradients in the supercage of Y zeolite by comparing the chemical shifts of ¹³¹Xe (I = 13/2) and ¹²⁹Xe (I = 1/2), *Stud. Surf. Sci. Catal.*, 2001, 135, p. 2341.
- [21] Moudrakovski I.L., Sanchez A., Ratcliffe C.I., Ripmeester J.A., Applications of hyperpolarized xenon to diffusion in vycor porous glass, *J. of Phys. Chem. B*, 2000, 104(31), p. 7306.
- [22] Moudrakovski I.L., Lang S., Ratcliffe C.I., Smard B., Santyr G., Ripmeester J.A., Chemical shift imaging with continuously flowing hyperpolarized xenon for the characterization of materials, *J. of Magnetic Resonance*, 2000, 144(2), p. 372.
- [23] Moudrakovski I.L., Wang L.Q., Baumann T., Satcher J.H., Exarhos G.J., Ratcliffe C.I., Ripmeester J.A., Probing the geometry and interconnectivity of pores in organic aerogels using hyperpolarized Xe-129 NMR spectroscopy, *JACS*, 2004, 126(16), p. 5052.
- [24] Conner W.C., Weist E.L., Ito T., Fraissard J., Characterization of the porous structure of agglomerated microspheres by xenon-129 NMR spectroscopy, *J. of Phys. Chem.*, 1989, 93, p. 4138.
- [25] Tersikh V.V., Moudrakovski I.L., Mastikhin V.M., ¹²⁹Xe nuclear magnetic resonance studies of the porous structure of silica gels, *J. Chem. Soc. Faraday Trans.*, 1993, 89(23), p. 4239.
- [26] Ripmeester J.A., Ratcliffe C.I., ¹²⁹Xe NMR spectroscopy in microporous solids: the effect of bulk properties, *Anal. Chim. Acta*, 1993, 283, p. 1103.
- [27] Tersikh V.V., Moudrakovski I.L., Breeze S.R., Lang S., Ratcliffe C.I., Ripmeester J.A., Sayari A., A general correlation for the Xe-129 NMR chemical shift-pore size relationship in porous silica-based materials, *Langmuir*, 2002, 18(15), p. 5653.
- [28] Kresge C.T., Leonowicz M.E., Roth W.J., Vartuli J.C., Beck J.S., Ordered mesoporous molecular sieves synthesized by a liquid-crystal template mechanism, *Nature*, 1992, 359, p. 710.
- [29] Springuel-Huet M.A., Fraissard J., Schmidt R., Stocker M., Conner W.C., Characterization of the porosity of M41S silicates by adsorption and Xe NMR, *Special Publications of the Royal Society of Chemistry*, 1997, 213, p. 452.
- [30] Springuel-Huet M.A., Sun K., Fraissard J., On the roughness of the internal surface of MCM-41 materials studied by Xe-129 NMR, *Microporous and Mesoporous Materials*, 1999, 33(1-3), p. 89.
- [31] Springuel-Huet M.A., Bonardet J.L., Gedeon A., Yue Y., Romannikov V.N., Fraissard J., Mechanical properties of mesoporous silicas and alumina-silicas MCM-41 and SBA-15 studied by N₂ adsorption and ¹²⁹Xe NMR, *Microporous and Mesoporous Materials*, 2001, 44 Special Iss. SI 77.
- [32] Nossov A., Haddad E., Guenneau F., Gedeon A., Continuous flow hyperpolarized ¹²⁹Xe-MAS NMR studies of microporous materials, *Phys. Chem. Chemical Phys.*, 2003, 5(20), p. 4479.
- [33] Guo W.P., Huang L.M., Deng P., Xue Z.Y., Li Q.Z., Characterization of Beta/MCM-41 composite molecular sieve compared with the mechanical

- mixture, *Microporous and Mesoporous Materials*, 2001, 44 Special Iss. SI 427.
- [34] Davidson A., Berthault P., Desvaux H., Silicas of unimodal and bimodal porosities probed by ^{129}Xe NMR spectroscopy, *J. of Phys. Chem. B*, 2003, 107(51), p. 14388.
- [35] Chen F., Zhang M.J., Han Y., Xiao F.S., Yue Y., Ye C.H., Deng F., Characterization of microporosity in ordered mesoporous material MAS-7 by ^{129}Xe NMR spectroscopy, *J. of Phys. Chem. B*, 2004, 108(12), p. 3728.
- [36] Nossov A., Haddad E., Guenneau F., Mignon C., Gedeon A., Grosso D., Babonneau F., Bonhomme C., Sanchez C., The first direct probing of porosity on supported mesoporous silica thin films through hyperpolarized ^{129}Xe NMR, *Chem. Comm.*, 2002, p. 2476.
- [37] Ryoo R., Ko C.H., Kim J.M., Howe R., Preparation of nanosize Pt clusters using ion exchange of $[\text{Pt}(\text{NH}_3)_4]^{2+}$ inside mesoporous channel of MCM-41, *Catalysis Letters*, 1996, 37(1-2), p. 29.
- [38] Filimonova S.V., Knicker H., Hausler W., Kogel K.L., ^{129}Xe NMR spectroscopy of adsorbed xenon as an approach for the characterization of soil meso- and microporosity, *Geoderma*, 2004, 122(1), p. 25.
- [39] Wang L.Q., Shin Y., Samuels W.D., Exarhos G.J., Moudrakovski I.L., Tersikh V.V., Ripmeester J.A., Magnetic resonance studies of hierarchically ordered replicas of wood cellular structures prepared by surfactant-mediated mineralization, *J. of Phys. Chem. B*, 2003, 107(50), p. 13793.
- [40] Gregory D.M., Gerald R.E., Boto R.E., Pore-structure determinations of silica aerogels by ^{129}Xe NMR spectroscopy and imaging, *J. of Magnetic Resonance*, 1998, 131(2), p. 327.
- [41] Pavlovskaya G., Blue A.K., Gibbs S.J., Haake M., Cros F., Mailer L., Meersmann T., Xenon-131 surface sensitive imaging of aerogels in liquid xenon near the critical point, *J. of Magnetic Resonance*, 1999, 137(1), p. 258.
- [42] Strange J.H., Rahman M., Characterization of porous solids by NMR, *Phys. Rev. Lett.*, 1993, 71, p. 3589.
- [43] Jackson C.L., McKenna G.B., The melting behavior of organic materials confined in porous solids, *J. Chem. Phys.*, 1990, 93, p. 9002.
- [44] Telkil V.-V., Lounila J., Jokisaari J., Behavior of acetonitrile confined to mesoporous silica gels as studied by ^{129}Xe NMR: a novel method for determining the pore sizes, *J. Phys. Chem. B*, 2005, 109, p. 757.
- [45] Saunavaara J., Jokisaari J., Xenon thermometer, to be published.
- [46] Tjandra N., Bax A., Direct measurement of distances and angles in biomolecules by NMR in a dilute liquid crystalline medium, *Science*, 1997, 278, p. 1111.
- [47] *Handbook of Liquid Crystals*, D. Demus, J. Goodby, G.W. Gray, H.-W. Spiess, V. Vill (eds), Wiley-VCH, Weinheim, 1998.
- [48] Bayle J.P., Courtieu J., Julien J., Étude RMN du xénon 129 dissous dans un mélange de cristaux liquides nématiques de faible anisotropie de susceptibilité magnétique, *J. Chim. Phys.*, 1987, 85, p. 147.
- [49] Cifelli M., Saunavaara J., Jokisaari J., Veracini C.A., ^{129}Xe nuclear shielding and diffusion in the A and C* phases of a chiral smectogen, *J. Phys. Chem.*, 2004, A108, p. 3973.
- [50] Ylihaata M., Lounila J., Jokisaari J., Nuclear magnetic shielding of noble gases in an anisotropic environment: ^{21}Ne and ^{129}Xe in a liquid crystal, *J. Chem. Phys.*, 1999, 110, p. 6381.
- [51] Jokisaari J., NMR of noble gases dissolved in liquids crystals, *NMR of ordered liquids*, E.E. Burnell, C.A. de Lange (eds), Kluwer, Dordrecht, 2003, p. 109.
- [52] Mansfield M., Flohr A., Veeman W.S., Application of ^{129}Xe NMR to polymer blends, *Appl. Magn. Reson.*, 1995, 8, p. 573.
- [53] Miller J.B., Walton J.H., Roland C.M., The NMR chemical shift of Xenon-129 dissolved in polymers, *Macromolecules*, 1993, 26, p. 5602.
- [54] Mansfield M., Veeman W.S., ^{129}Xe NMR exchange spectroscopy for probing the microstructure of porous materials, *Chem. Phys. Lett.*, 1993, 213, p. 153.
- [55] Junker F., Veeman W.S., Xenon self-diffusion in organic polymers by pulsed field gradient NMR, *Macromolecules*, 1998, 31, p. 1485.
- [56] Lühmer M., Reisse J., Quadrupole NMR relaxation of the noble gases dissolved in simple liquids and solutions. A critical review of experimental data in the light of computer simulation results, *Progr. Nucl. Magn. Res. Spectr.*, 1998, 33, p. 57.
- [57] Lühmer M., Moschos A., Reisse J., Intermolecular dipole-dipole spin relaxation of xenon-129 dissolved in benzene. A molecular-dynamics simulation study, *J. Magn. Res. Series A*, 1995, 113, p. 164.
- [58] Lühmer M., Goodson B.M., Song Y.-Q., Laws D.D., Kaiser L., Cyrier M.C., Pines A., Study of xenon binding in cryptophane-A using laser-induced NMR polarization enhancement, *J. Am. Chem. Soc.*, 1999, 121, p. 3502.
- [59] Song Y.Q., Goodson B.M., Taylor R.E., Laws D.D., Navon G., Pines A., Selective enhancement of NMR signals for alpha-cyclodextrin with laser-polarized xenon, *Angew. Chem. Int. Ed. Engl.*, 1997, 36, p. 2368.
- [60] Dubois L., Parrès S., Huber J.G., Berthault P., Desvaux H., Dynamics of xenon inside hydrophobic cavities as probed by NMR relaxation of dissolved laser-polarized xenon, *J. Phys. Chem. B*, 2004, 108, p. 767.
- [61] Locci E., Casu M., Saba G., Lai A., Reisse J., Bartik K., The potential of ^{129}Xe NMR relaxation measurements for the study of heme proteins, *ChemPhysChem*, 2002, 3(9), p. 812.
- [62] Silth A., Hitchens T.K., Hinton D.P., Berr S.S., Driehuys B., Brookeman J.R., Bryant R.G., Consequences of ^{129}Xe - ^1H cross relaxation in aqueous solutions, *J. Magn. Res.*, 1999, 139, p. 225.
- [63] Lühmer M., Dejaegere A., Reisse J., Interpretation of the solvent effect on the Screening constant of Xe-129, *Magn. Res. Chem.*, 1989, 27, p. 950.
- [64] Bartik K., Lühmer M., Dutasta J.P., Collet A., Reisse J., ^{129}Xe and ^1H NMR study of the reversible trapping of xenon by cryptophane-A in organic solution, *J. Am. Chem. Soc.*, 1998, 120, p. 784.
- [65] Branda N., Grotzfeld R.M., Valdes C., Rebek J., Control of self-assembly and reversible encapsulation of xenon in a self-assembling dimer by acid-base chemistry, *J. Am. Chem. Soc.*, 1995, 117, p. 85.
- [66] Robbins T.A., Knobler C.B., Bellow D.R., Cram D.J., Host-guest complexation. A highly adaptive and strongly binding hemiacetate, *J. Am. Chem. Soc.*, 1994, 116(1), p. 111.
- [67] Bartik K., Lühmer M., Heyes S.J., Ottinger R., Reisse J., Probing molecular cavities in α -cyclodextrin solutions by xenon NMR, *J. Magn. Res. Series*, 1995, 109, p. 164.
- [68] Ripmeester J.A., Ratcliffe C.I., Tse J.S., The nuclear magnetic resonance of ^{129}Xe trapped in clathrates and some other solids, *J. Chem. Soc. Faraday Trans. 1*, 1988, 84(11), p. 3731.
- [69] Broth T., Devic T., Lesage A., Emsley L., Collet A., Synthesis of deuterium-labeled cryptophane-A and investigation of Xe@cryptophane complexation dynamics by 1D-EXSY NMR experiments, *Chem. Eur. J.*, 2001, 7(7), p. 1561.
- [70] Bartik K., Lühmer M., Collet A., Reisse J., Molecular polarization and molecular chiralization: the first example of a chiralized xenon atom, *Chirality*, 2001, 13, p. 2.
- [71] Landon C., Berthault P., Vovelle F., Desvaux H., Magnetization transfer from laser-polarized xenon to protons located in the hydrophobic cavity of the wheat non specific lipid transfer protein, *Prot. Sci.*, 2001, 10, p. 762.
- [72] Tilton R.F.J., Kuntz I.D.J., Nuclear magnetic resonance studies of xenon-129 with myoglobin and hemoglobin, *Biochemistry*, 1982, 21, p. 6850.
- [73] Rubin S.M., Spence M.M., Goodson B.M., Wemmer D.E., Pines A., Evidence of nonspecific surface interactions between laser-polarized xenon and myoglobin in solution, *Proc. Natl. Acad. Sci. U.S.A.*, 2000, 97, p. 9472.
- [74] Locci E., Dehouck Y., Casu M., Saba G., Lai A., Lühmer M., Reisse J., Bartik K., Probing proteins in solution by ^{129}Xe NMR spectroscopy, *J. Magn. Res.*, 2001, 150, p. 167.
- [75] Schoenborn B. P., Watson H. C., Kendrew J. C., Binding of Xenon to Spem Whale Myoglobin, *Nature*, 1965, 207, p. 28.
- [76] Locci E., Reisse J., Bartik K., The Potential of the Xenon "Spin-Spy" Methodology for the Study of Configurational Equilibria in Solution, *ChemPhysChem*, 2003, 4(3), p. 305.
- [77] Locci E., Bartik K., Segebarth N., Lühmer M., Reisse J., Stereochemical Studies by Molecular Palpation, *J. Phys. Org. Chem.*, 2004, 17, p. 787.
- [78] Tse S.D., Anthenien R.A., Fernandez-Pello A.C.K.M., An application of ultrasonic tomographic imaging to study smoldering combustion, *Combustion and Flame*, 1999, 116, p. 120.
- [79] Moule A.J., Spence M.M., Han S.-I., Seeley J.A., Pierce K.L., Saxena S., Pines A., Amplification of xenon NMR and MRI by remote detection, *Proc. Natl. Acad. Sci. USA*, 2003, 100(16), p. 9122.
- [80] Greenberg Y.S., Application of superconducting quantum interference devices to nuclear magnetic resonance, *Rev. Mod. Phys.*, 1998, 70(1), p. 175.
- [81] Yashchuk V.V., Granwehr J., Kimball D.F., Rochester S.M., Trabesinger A.H., Urban T.J., Budker D., Pines A., Atomic magnetometry for detection of nuclear magnetization, *Phys. Rev. Lett.*, 2004, 93, p. 160801.
- [82] Raftery D., Long H.W., Shykld D., Grandinetti P.J., Pines A., Multi-pulse NMR of optically-pumped xenon in a low magnetic field, *Phys. Rev.*, 1994, A50, p. 567.
- [83] Seeley J.A., Han S.-I., Pines A., Remotely detected high-field MRI of porous samples, *J. Magn. Res.*, 2004, 167, p. 282.
- [84] Lowery T.J., Rubin S.M., Ruiz E.J., Spence M.M., Winsinger N., Schultz P.G., Pines A., Wemmer D.E., Application of laser-polarized ^{129}Xe to biomolecular assays, *Magn. Res. Imag.*, 2003, 21, p. 1235.
- [85] Rubin S.M., Spence M.M., Goodson B.M., Wemmer D.E., Pines A., Evidence of nonspecific surface interaction between laser-polarized xenon and myoglobin in solution, *Proc. Natl. Acad. Sci. USA*, 2000, 97, p. 9472.
- [86] Rubin S.M., Lee S.-Y., Ruiz E.J., Pines A., Wemmer D.E., Detection and characterization of xenon-binding sites in proteins by ^{129}Xe NMR spectroscopy, *J. Mol. Biol.*, 2002, 322, p. 425.
- [87] Lowery T.J., Rubin S. M., Ruiz E.J., Pines A., Wemmer D., Design of a conformation-sensitive xenon-binding cavity in the ribose-binding protein, *Angewandte Chemistry*, 2004, 43(46), p. 6320.
- [88] Spence M.M., Ruiz E.J., Rubin S.M., Lowery T.J., Winsinger N., Schultz P.G., Wemmer D.E., Pines A., Development of a functionalized xenon biosensor, *JACS*, 2004, 126, p. 15287.
- [89] Oros A.M., Shah N.J., Hyperpolarized xenon in NMR and MRI, *Phys. Med. Biol.*, 2004, 49, p. F105.
- [90] Duhamel G., Choquet P., Grillon E., Lamalle L., Levell J.L., Ziegler A., Constantinesco A., Xenon-129 MR imaging and spectroscopy of rat brain using arterial delivery of HP xenon in a lipid emulsion, *Magn. Reson. Med.*, 2001, 46, p. 208.

Article soumis le 03/12/2004, accepté le 12/04/2005.



From left to right and from top to bottom:

Jacques Fraissard, professor « Émérite » at the University P. and M. Curie, Paris (France)¹, has coordinated this paper, **Kristin Bartik**, professor at the Université Libre de Bruxelles (Belgium)², **Philippe Choquet**, « maître de conférences » at the University Hospital of Strasbourg (France)³, **Guillaume Duhamel**, researcher at the « Centre de Résonance Magnétique Biologique et Médicale » of Marseille (France)⁴, **Jean-Noël Hyacinthe**, PhD student at the Université Joseph Fourier (France)⁵, **Jukka Jokisaari**, professor at the University of Oulu (Finland)⁶, **Emanuela Locci**, doctor at the Università di Cagliari (Italy)⁷, **Thomas J. Lowery**, professor at the University of California, Berkeley (USA)⁸, **Michel Luhmer**, professor at the Université Libre de Bruxelles (Belgium)⁹, **Thomas Meersmann**, professor at the Colorado State University, Fort Collins (USA)¹⁰, **Igor L. Moudrakovski**, senior research council officer at the Steacie Institute for Molecular Sciences, Ottawa (Canada)¹¹, **Galina E. Pavlovskaya**, postdoc at the Colorado State University (USA)¹⁰, **Kimberly L. Pierce**, PhD student at the University of California, Berkeley (USA)¹², **Alexander Pines**, professor at the University of California, Berkeley (USA)¹², **John A. Ripmeester**, principal officer at NRC, Steacie Institute for Molecular Sciences, Ottawa (Canada)¹¹, **Ville-Veikko Telkki**, master of sciences at the University of Oulu (Finland)⁶, **Wibren S. Veeman**, professor at the Duisben-Essen Universität in Germany¹³.

¹ University Pierre and Marie Curie, Laboratoire PMMH, ESPCI, 10 rue Vauquelin, 75231 Paris (France).
E-mail: jfr@ccr.jussieu.fr

² Molecular and Biomolecular Engineering, CP 165/64, Université Libre de Bruxelles (Belgium).

³ Service de Biophysique et Médecine Nucléaire, CHU Haute-pierre, Strasbourg, (France).

⁴ INSERM, Neuroimagerie Fonctionnelle et Métabolique, Université Joseph Fourier, CHU-Pavillon B, Grenoble (France).

⁵ Centre de Résonance Magnétique Nucléaire et Médicale CNRS-UMR 6612, Marseille (France).

⁶ NMR Research Group, Department of Physical Sciences, FIN-90014 University of Oulu (Finland).

⁷ Dipartimento di Scienze Chimiche, Università di Cagliari (Italy).

⁸ Physical Biosciences Division, Lawrence Berkeley National Laboratory, and Department of Chemistry, University of California, Berkeley, CA 94720 (USA).

⁹ Laboratoire de RMN Haute Résolution, CP 160/08, Université Libre de Bruxelles, (Belgium).

¹⁰ Department of Chemistry, Colorado State University, Fort Collins, CO 80523 (USA).

¹¹ Steacie Institute for Molecular Sciences, National Research Council Canada, Ottawa, Ontario (Canada).

¹² Materials Science Division, Lawrence Berkeley National Laboratory, and Department of Chemistry, University of California, Berkeley, CA 94720 (USA).

¹³ Universität Duisburg-Essen (Germany).

Depuis 1988

Les Editions D'Ile de France



Expérience,
la différence

PUBLICATION
REVUE PUBLICITAIRE
EDITION
FINANCEMENT

Notre société est spécialisée dans l'édition d'annuaires et de revues professionnelles pour sociétés savantes, associations d'élèves d'écoles d'ingénieurs, fédérations professionnelles.

Notre présence depuis plus de 17 ans dans un secteur d'activités en mutation permanente, la transparence de nos résultats régulièrement positifs depuis la création de notre société, la fidélité de nos partenaires éditoriaux, sont autant de preuves de professionnalisme, de notre équité et confortant de fait notre renommée, carte de visite.

Notre autre atout majeur, et c'est aussi notre spécialité, est de vous garantir et gratuitement des pages publiées en concordance de l'exclusivité de la revue publicitaire édité et diffusée par notre réseau commercial.

Editeur exclusif
de la Revue l'ACTUALITE CHIMIQUE

Editions D'Ile de France

102, avenue Georges Clemenceau • 91700 Malesherbes

Tél. : 33 1 43 53 64 00 • Fax : 33 1 43 53 48 00

e-mail : edition@edif.fr

www.edif.fr

